



**NIST Interagency Report
NIST IR 8550**

Spectral Characteristics and Indoor Air Quality Effects of Germicidal 254 nm and 222 nm Ultraviolet Light

Michael F. Link
Andrew Shore
Rleigh Robertson
Behrang H. Hamadani
Dustin Poppendieck

This publication is available free of charge from:
<https://doi.org/10.6028/NIST.IR.8550>

**NIST Interagency Report
NIST IR 8550**

Spectral Characteristics and Indoor Air Quality Effects of Germicidal 254 nm and 222 nm Ultraviolet Light

Michael F. Link
Andrew Shore
Rileigh Robertson
Behrang H. Hamadani
Dustin Poppendieck
*Building Energy and Environment
Division/Engineering Laboratory*

This publication is available free of charge from:
<https://doi.org/10.6028/NIST.IR.8550>

November 2024



U.S. Department of Commerce
Gina M. Raimondo, Secretary

National Institute of Standards and Technology
Laurie E. Locascio, NIST Director and Under Secretary of Commerce for Standards and Technology

NIST IR 8550
November 2024

NIST Technical Series Policies

[Copyright, Use, and Licensing Statements](#)

[NIST Technical Series Publication Identifier Syntax](#)

Publication History

Approved by the NIST Editorial Review Board on 2024-11-26

How to Cite this NIST Technical Series Publication

Link MF, Shore A, Robertson R, Hamadani BH, Poppendieck D (2024) Spectral Characteristics and Indoor Air Quality Effects of Germicidal 254 nm and 222 nm Ultraviolet Light. (National Institute of Standards and Technology, Gaithersburg, MD), NIST Internal Report (IR) NIST IR 8550. <https://doi.org/10.6028/NIST.IR.8550>

Author ORCID iDs

Michael F. Link: 0000-0002-1841-2455

Andrew Shore: 0000-0002-1860-1600

Raleigh Robertson: none

Behrang H. Hamadani: 0000-0002-2410-9444

Dustin Poppendieck: 0000-0002-1100-511X

Contact Information

Michael Link: michael.f.link@nist.gov

Abstract

Current Germicidal Ultraviolet (GUV) devices are designed to inactivate pathogens in air at either 222 nm or 254 nm wavelengths. Previous research has demonstrated both wavelengths can produce oxidants in air (222 nm: ozone, 254 nm: hydroxyl radicals) and potentially directly photolyze some chemicals. This study sought to determine the impacts of GUV devices on indoor air chemistry in both laboratory chamber and field settings.

To ensure the devices were operating using wavelengths and intensities of interest, spatial spectral irradiance measurements of one 222 nm (GUV222) and one 254 nm (GUV254) device were performed. Chamber testing to determine air quality impacts consisted of operating the above devices for four hours in a sealed chamber containing six challenge chemicals. Field testing consisted of operating the devices in an unoccupied restroom on the campus of the National Institute of Standards and Technology (NIST). Ozone, formaldehyde, other volatile organic compound (VOC) oxidation products and ultrafine particles were measured for each device in both the chamber and restroom.

In chamber experiments GUV254 generated formaldehyde and likely directly photolyzed an equivalent amount of acetone, contributing to a minimal net change in VOC oxidation products. In addition, GUV254 generated measurable ultrafine particles in the chamber experiments, albeit less than GUV222. For GUV254, formaldehyde, VOC oxidation products, ultrafine particles and ozone generation were not measurable in the restroom.

In both the chamber and restroom installation GUV222 generated ozone, VOC oxidation products and ultrafine particles. GUV222 generated quantifiable formaldehyde in chamber testing only. GUV222 was demonstrated to directly photolyze tetrachloroethylene in the chamber.

Lastly, to better understand the irradiance spectrum in indoor spaces where GUV devices may be deployed, spatial and temporal changes to the 375 nm to 850 nm spectrum were examined at the NIST Net-Zero Energy Residential Test Facility (NZERTF). A measurement location near a window was compared to one close to an interior ceiling. Indoor diurnal total irradiance and spectrums collected near the spring equinox and summer solstice were compared.

This work was funded by the U. S. Environmental Protection Agency via contract DW1392571901.

Keywords

Germicidal Ultraviolet (GUV) devices, Ozone, Ultrafine Particles, Formaldehyde, Volatile organic chemical (VOC) oxidation products

Table of Contents

1. Disinfection and Indoor Air Quality Impacts with Germicidal Ultraviolet Light (GUV)	6
1.1. 254 nm GUV Chemistry and Disinfection.....	6
1.2. 222 nm GUV Chemistry and Disinfection.....	6
1.3. Mechanisms and Implications of GUV254 and GUV222 Air Chemistry.....	7
1.3.1. GUV254 Chemistry.....	7
1.3.2. GUV222 Chemistry.....	8
1.3.3. Differences Between GUV254 and GUV222 Chemistry.....	9
2. Characterization of GUV Spectral Irradiance	11
2.1. Test Design: Spatial Spectral Irradiance Measurements.....	11
2.2. GUV254 Lamp Emission.....	12
2.3. GUV222 Lamp Emission.....	13
3. Air Quality Impacts from GUV Operation in Laboratory Tests	15
3.1. Laboratory Test Design: ASTM Method WK81750.....	15
3.2. Byproduct Formation from GUV Under Test Conditions.....	17
3.2.1. O ₃ Generation from GUV254.....	17
3.2.2. O ₃ Generation from GUV222.....	17
3.2.2.1. Estimating the GUV222 Fluence Rate Using Three Different Methods.....	18
3.2.3. VOC Byproduct Formation from GUV254 and GUV222.....	19
3.2.4. Particulate Matter Formation.....	20
3.2.5. Evidence for VOC Photolysis from GUV254 and GUV222.....	21
4. Air Quality Impacts from GUV Operation in a Restroom	23
4.1. Restroom Installation Experiment Design.....	23
4.2. GUV254 in the Restroom.....	24
4.3. Air Quality Impacts from GUV222 in the Restroom.....	24
4.3.1. Generation of O ₃ , VOC Oxidation Products from O ₃ Chemistry, and Particulate Matter.....	24
4.3.2. VOC Oxidation Products from O ₃ Chemistry (VOC _{O₃ ox.}).....	27
4.3.3. Ultrafine Particle Generation.....	28
4.3.4. Aerosol Mass Generation.....	28
5. Solar Influenced Irradiance Data	30
5.1. Indoor Spatial and Temporal Total Irradiance.....	30
5.2. Indoor Spatial and Temporal Total Irradiance Data Files.....	31
6. Summary and Conclusions	32
References	33
A. Appendix	36

List of Tables

Table 1	Horizontal and Vertical Increments for Spatial Lamp Irradiance Measurements.....	12
Table 2.	Room-averaged fluence rates determined from three different methods.	19
Table 3.	Quantifiable GUV impacts on indoor chemistry.	32

List of Figures

Figure 1.	Calculation of O ₃ production (left, pink) and destruction (right, black) rate (nmol mol ⁻¹ h ⁻¹). From left to right the background is shaded blue for the UVC, peach for the UVB, and gray for the UVA regions of the electromagnetic spectrum. Blue vertical dashed lines show where the product and destruction curves intersect the primary emission wavelengths from GUV222 (left, 222 nm) and GUV254 (right, 254 nm).	9
Figure 2.	Robotic arm with integrating sphere and calibrated spectrometer assembly set up to measure spectral irradiance from GUV254 lamp. Set up was similar for GUV222 lamp. Coordinate system for the robot is shown.	11
Figure 3.	Bounded irradiance of 254 nm lamp measured in planes of a) 0 cm, b) 1 cm, c) 5 cm, d) 10 cm, e) 20 cm, f) 50 cm, and g) 100 cm from source. Irradiance values are integrated over 250 nm to 257 nm to capture emission at 254 nm. Irradiance color bar is unique for each distance. To visualize irradiance decay over distance with a constant irradiance color bar see Figure A.1.	13
Figure 4.	Bounded Irradiance from KrCl 222 nm source measured in planes of a) 0 cm, b) 1 cm, c) 5 cm, d) 10 cm, e) 20 cm, f) 50 cm, and g) 100 cm from source. Irradiance values are integrated over 205 nm to 235 nm which gives the total emission of the lamp. Irradiance color bar is unique for each distance. To visualize irradiance decay over distance with a constant irradiance color bar see Figure A.2.	14
Figure 5.	The 31.5 m ³ environmentally controlled chamber used for quantifying air byproduct formation from GUV devices. Red lines indicate VOC (left) and particle (right) sampling lines. Pink lines shown chemical (left) and particle (right) injection lines. The GUV222 device is shown pointed down towards the center of the room on the left and the GUV254 device is shown illuminating the upper part of the space on the right.....	15
Figure 6.	Concentration decay of select challenge chemicals observed during Test 1. [X] is the concentration of a challenge chemical. k _{decay} is the slope of a linear fit of the natural log of the chemical concentration as a function of time divide by the initial chemical concentration compared to time. The concentration data and fits for all chemicals other than limonene, O ₃ , and ultrafine particle (UFP) are indistinguishable from each other at this scale and represented by the black HCHO line. Note: Uncertainty in k _{decay} was less than 6 % for any given linear fit determination whereas variability of k _{decay} between replicate tests was within 20 %.	16
Figure 7.	O ₃ generated from GUV222 measured (black solid line) during seven replicates of Test 2. Two model predictions of O ₃ generation are shown where the fluence rate was estimated from spectral irradiance measurements (yellow dashed line) and using PERC as an actinometer (blue dashed). Purple dots show that O ₃ was not generated when the light output was covered.	17
Figure 8.	Speciated VOC concentrations measured during Test 2 for GUV222 and GUV254.	19

Figure 9. Net VOC concentration change during Test 2 for GUV222 and GUV254. Uncertainty for GUV222 is shown via shaded region. Uncertainty ($\pm 25\%$ from propagation of calibration uncertainties) for GUV254 is not visible at this scale. 20

Figure 10. Ultrafine particle production from GUV222 and GUV254. Top panels show total number concentrations. Bottom panels show the particle diameter specific concentrations. Each panel has a different scale..... 21

Figure 11. (a) Picture of GUV254 installation in restroom. (b) Diagram of restroom GUV installations and experiment. (c) Picture of GUV222 installation in restroom..... 23

Figure 12. The air change rate in Wk1 was about 1 h^{-1} . Byproducts include O_3 (blue), VOC O_3 oxidation products ($\text{VOC}_{\text{O}_3\text{ Ox.}}$, black), particle number (N_p , red), and particle mass (M_p , green) concentrations. Pink shaded regions show when GUV222 was on. Blue shaded regions show when GUV254 was on. Dotted lines indicate the 8-hour periods where a mixing fan was on. Shaded areas below the traces show the estimated increase in byproduct concentrations generated by GUV222. Hallway concentrations of VOC O_3 oxidation products ($\text{VOC}_{\text{O}_3\text{ Ox.}}$) and O_3 are used in O_3 and $\text{VOC}_{\text{O}_3\text{ Ox.}}$ generation rate calculations. A decrease in O_3 concentrations (dark blue for restroom and light blue for hallway) with increased NO (orange) concentrations is shown. $\text{VOC}_{\text{O}_3\text{ Ox.}}$ is the sum of 34 VOCs observed to increase in concentration when GUV222 was turned on. The y-axis for particle number is the particle number divided by 1000. The uncertainty in O_3 concentrations is $\pm 0.3\text{ nmol mol}^{-1}$. The uncertainty in $\text{VOC}_{\text{O}_3\text{ Ox.}}$ is $\pm 25\%$. The uncertainty in particle number concentrations is $< 1\%$, but the conversion of particle number concentrations to aerosol mass carries an uncertainty of 10% from the SOA density estimate..... 25

Figure 13. The ACR in Wk2 was about 2 h^{-1} . The descriptions in the caption for Figure 12 apply to this figure also. A MERV-13 do-it-yourself (DIY) air cleaner was used for two GUV222 on/off cycles at the end of the weekend (teal dotted lines and dots). 26

Figure 14. Average time series of $\text{VOC}_{\text{O}_3\text{ Ox.}}$ produced from GUV222 during Wk1 and Wk2..... 27

Figure 15. Ultrafine particle number concentrations (top, note different scales) for Wk1 (left) and Wk2 (right) with lognormal number size distributions ($dN/d\log D_p$; bottom)..... 28

Figure 16. Aerosol mass production predicted from measurements of laboratory-determined secondary organic aerosol (SOA) yields compared to what was measured in Wk1. First two bars are predicted from reacted VOC concentrations and published SOA yields. The third bar is what was measured. 29

Figure 17. Total irradiance in the living room of NIST's Net-Zero Energy Residential Test Facility (NZERTF) at a) a south facing window and b) 50 cm under a recessed ceiling LED. Irradiance is reported on a day near the spring equinox (3/21) and a day near the summer solstice (6/22). Note that the roof overhang at the NZERTF reduces solar radiation incident on the windows during the summer and maximizes it during the winter months. LED lights turn on at time 17.5 h after midnight, which account for the peaks on the interior plot (right, note the difference in scale). 30

Figure 18. Measured spectral irradiance at various locations. The maximum irradiance due to solar radiation is shown in a) for outdoor conditions at peak irradiance near the spring equinox and summer solstice as well as on a peak day in spring equinox in the living room at a south facing window. This indoor window spectrum is also compared in b) to indoor spectra at night under the recessed LED and a peak measurement during the day while the LED is off. 31

Figure A.1. Bounded Irradiance of 254 nm lamp measured in planes of a) 0 cm, b) 1 cm, c) 5 cm, d) 10 cm, e) 20 cm, f) 50 cm, and g) 100 cm from source. Irradiance values are integrated over 250 nm to 257 nm to capture emission at 254 nm. Irradiance color bar is kept constant for all measurements. 36

Figure A.2. Bounded Irradiance from KrCl 222 nm source measured in planes of a) 0 cm, b) 1 cm, c) 5 cm, d) 10 cm, e) 20 cm, f) 50 cm, and g) 100 cm from source. Irradiance values are integrated over 205 nm to 235 nm which gives the total emission of the lamp. Irradiance color bar is kept constant for all measurements..... 37

1. Disinfection and Indoor Air Quality Impacts with Germicidal Ultraviolet Light (GUV)

With the onset of the COVID-19 pandemic, challenges associated with mitigating airborne virus transmission in public spaces motivated the development of new ventilation and disinfection standards in the United States [1]. One important example is ASHRAE Standard 241-2023 “Control of Infectious Aerosols.” Standard 241 prescribes minimum effective clean airflow rates on a per-person basis when the system is in an infection risk management mode [2]. These clean airflow rates can be achieved using a combination of mechanical ventilation and air disinfection technologies. Germicidal ultraviolet lights (GUV) are one such technology. GUV with peak emission wavelengths at 254 nm (GUV254) or 222 nm (GUV222) have been promoted as possible airborne pathogen transmission mitigation tools. GUV222 possibly can efficiently deactivate airborne viruses [3-6] and directly irradiate human occupied indoor spaces—potentially without causing harm to skin or eyes [7-9]. GUV254 has a history of demonstrated efficacy for a range of pathogens [10-12], but harm to indoor occupants from improper installation is one possible practical limitation.

Alongside the renewed consideration of GUV technologies for pathogen control, an interest in the possible air chemistry and formation of undesirable air byproducts resulting from ultraviolet irradiation of air and surfaces has also emerged [13,14]. Limited laboratory and real-world experimental evidence exist demonstrating if, where, and when GUV technologies may generate undesirable air byproducts. Useful operational guidance is also limited by an incomplete understanding of how spectral output is quantified combined with an incomplete understanding of how much output is needed to deactivate airborne pathogens while minimizing the potential formation of air byproducts.

1.1. 254 nm GUV Chemistry and Disinfection

GUV254 has a history of both laboratory and field demonstrated efficacy against deactivating airborne pathogens [15-17]. However, one major drawback to GUV254 is that skin and eye damage can occur if human occupants are directly irradiated. Potential air quality impacts from GUV254 were first postulated by Peng, et al. [13] and at least one modeling study has concluded the formation of unintended air byproducts are possible from installation of GUV254 in a classroom [14]. Limited measurements of gaseous and particulate matter air byproducts exist from a laboratory study [18] and a study of a GUV254 device in an academic laboratory [19].

1.2. 222 nm GUV Chemistry and Disinfection

GUV222 has recently emerged in the past five years as a potentially valuable tool for combating airborne pathogen transmission [4,20]. The advantage of GUV222 compared to GUV254 is in the potential ability to irradiate human occupants directly without causing skin or eye damage [21]. Currently, there is considerable uncertainty concerning how much radiation (i.e., dose rate or fluence rate) is needed for effective deactivation of airborne pathogens at this wavelength.

One concerning aspect of GUV222 is that the UV light generates ozone (O_3), an indoor air pollutant, in the presence of air [22]. When indoors, O_3 reacts rapidly with surfaces, sometimes forming gaseous byproducts, and can react with VOCs in the gas-phase to form particulate matter byproducts. O_3 is undesirable indoors because it is linked to adverse health outcomes possibly through the formation of secondary gaseous or particulate matter byproducts [23,24]. The amount of O_3 formed from a GUV222 device is strongly dependent on the fluence rate. Thus, standard GUV222 fluence rates for effective deactivation are needed for risk assessment as the fluence rate will determine how much O_3 may possibly form indoors.

1.3. Mechanisms and Implications of GUV254 and GUV222 Air Chemistry

1.3.1. GUV254 Chemistry

Unintended air byproducts can be generated from GUV254 following two known pathways: (1) generation of hydroxyl radical (OH) and (2) direct photolysis of gaseous inorganic species and volatile organic compounds (VOCs).

OH can be generated from photolysis of O_3 in the presence of water vapor (Reaction 1 and Reaction 2).



In Reaction 1 O_3 absorbs a photon ($h\nu$) of wavelength less than 330 nm. This photolyzing results in an oxygen atom excited to the singlet electronic state ($O(^1D)$). Most of the $O(^1D)$ is collisionally quenched to form a ground state oxygen atom ($O(^3P)$) which then rapidly reacts with oxygen in a termolecular reaction (where M represents a collisional body, N_2 or O_2) to reform O_3 . However, a fraction of the $O(^1D)$ (about 10 % of the $O(^1D)$ at 30 % relative humidity) will react with water vapor to form two OH.

The rate of O_3 photolysis from 254 nm light is described by Equation (1),

$$\frac{d[O_3]}{dt} = -j_{O_3}[O_3] \quad (1)$$

where j_{O_3} is the first-order O_3 photolysis rate constant (s^{-1}) and $[O_3]$ is the O_3 concentration (molecules cm^{-3}). j_{O_3} is calculated by integrating across the range of relevant wavelengths following Equation (2),

$$j_{O_3} = \int \sigma_{O_3} \Phi_{O_3} F d\lambda \quad (2)$$

where σ_{O_3} is the O_3 absorption cross section (cm^2), Φ_{O_3} is the O_3 photolysis quantum yield, and F is the photon flux (quanta cm^{-2}). For GUV light sources the photon flux can be calculated from reported fluence rates ($\mu W \text{ cm}^{-2}$) through unit conversions. Typical room-averaged fluence rates for GUV254 are approximately $50 \mu W \text{ cm}^{-2}$. Photochemical properties like absorption

cross sections and quantum yields can be found in a data compilation prepared by the National Aeronautics and Space Administration (NASA) Panel for Data Evaluation [25].

Photolysis of VOCs containing the carbonyl (C=O bond) chromophore, following electronic transition of π -bonded electrons, can occur from absorption of 254 nm light and result in unintended air byproducts. Considerable laboratory measurements of organic and inorganic radical production from VOC photolysis exist in the literature, and notable carbonyl-containing VOCs like acetone, methyl ethyl ketone, and 2,3-butadione, that have been reported in indoor air samples, have absorption cross sections that peak around 254 nm [26].

1.3.2. GUV222 Chemistry

Unintended air byproducts can be generated from GUV222 following two known pathways: (1) photolysis of oxygen (O_2), and subsequent reactions, of O_3 and (2) direct photolysis of gaseous inorganic species and VOCs.

O_3 can be generated from photolysis of O_2 at 222 nm forming two ground state oxygen atoms (Reaction 1) that then can combine with molecular oxygen to form ozone (Reaction 2).



The rate of O_3 production from 222 nm light is described by Equation (3),

$$\frac{d[O_3]}{dt} = j_{O_2}[O_2] \quad (3)$$

where j_{O_2} is the first-order O_2 photolysis rate constant (s^{-1}) and $[O_2]$ is the O_2 concentration (molecules cm^{-3}). $[O_2]$ is approximately equal to 5×10^{18} molecules cm^{-3} at standard temperature and pressure. At pressures typical indoors, where GUV222 is likely to be applied, the photochemical loss of ozone from the 222 nm wavelength is negligible so we do not address that here. j_{O_2} is calculated similar to j_{O_3} described above, but further details can be found in Link, et al. [22]. In application, typical room-averaged fluence rates for GUV222 span a wide range between $0.1 \mu W \text{ cm}^{-2}$ [27] and $5 \mu W \text{ cm}^{-2}$ [28], though methods of determining fluence rate values are inconsistent and values required for pathogen inactivation are still being determined.

Limited experimental evidence has demonstrated photolysis of VOCs from GUV222. Recently, GUV222 has been demonstrated to photolyze lactic acid to form acetaldehyde among other products [30]. In addition, $C_2H_5O_2^+$ and $C_4H_9^+$ ions (potentially representing acetic acid and butanol respectively) were detected in a room where GUV222 ozone was scavenged with OH, indicating they were formed from direct 222 nm photooxidation of gaseous VOCs or surfaces [29]. Although experimental evidence is limited, some inorganic species like nitrogen dioxide and hypochlorous acid (HOCl) have enhanced absorption cross sections at 222 nm [25] and may be present in indoor air from outdoor air intrusions, unventilated combustion, or cleaning and potentially lead to unintended air chemistry.

1.3.3. Differences Between GUV254 and GUV222 Chemistry

There are key differences in the air chemistry that can result from GUV254 and GUV222 operation and thus differences on their impact to indoor air quality. Both technologies can generate oxidants, with GUV222 generating O_3 and GUV254 generating OH from the destruction of O_3 . Figure 1 shows the O_3 production and destruction rate as a function of wavelength. For the production rate calculation, a uniform fluence rate of $2 \mu W cm^{-2}$ (typical for 222 nm applications) across the 200 nm to 400 nm range is used to demonstrate the influence of the O_2 action spectrum (i.e., the product of the O_2 absorption cross section and photolysis quantum yield) on O_3 production. For the destruction rate calculation, a uniform fluence rate of $50 \mu W cm^{-2}$ (typical for 254 nm applications) was used to demonstrate the influence of the O_3 action spectrum on O_3 photolysis.

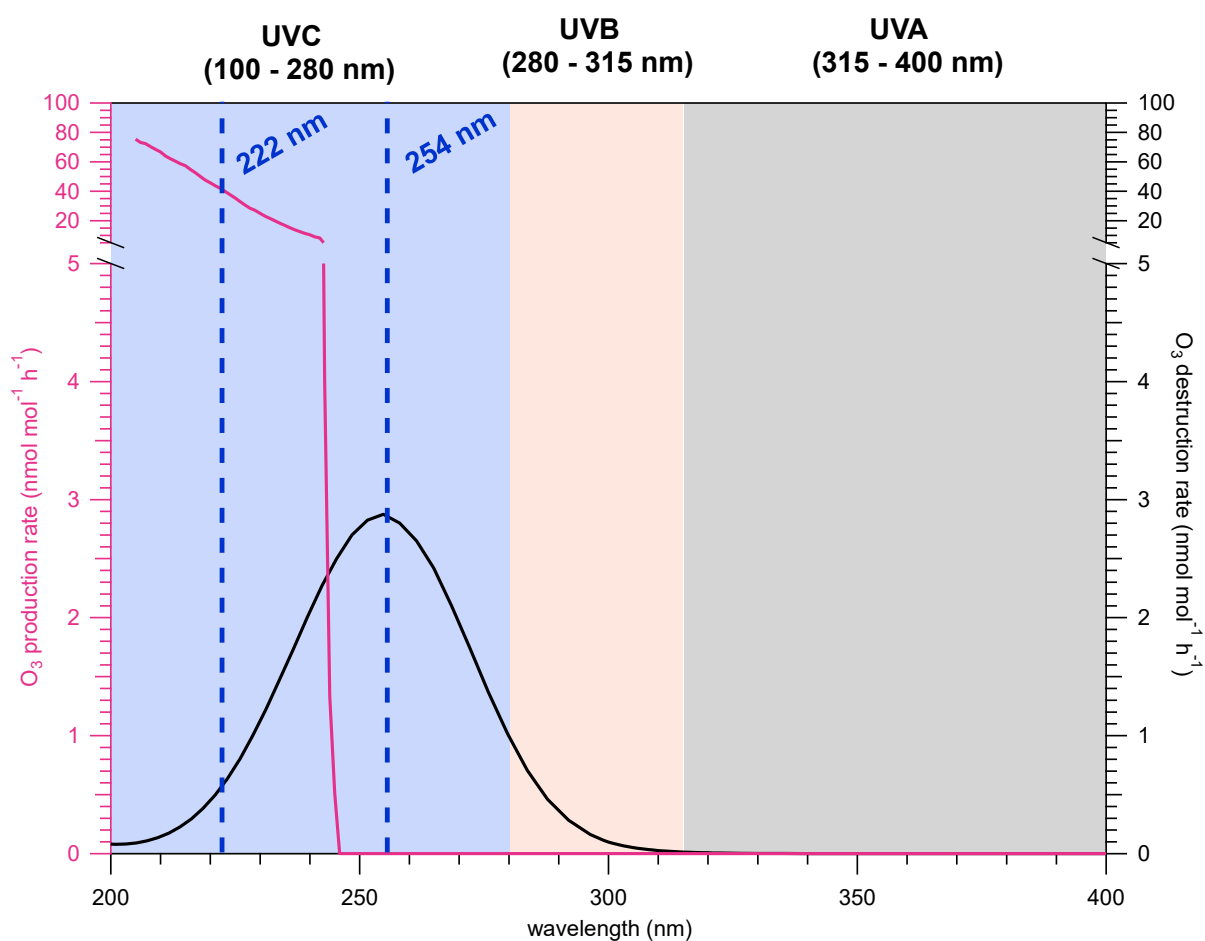


Figure 1. Calculation of O_3 production (left, pink) and destruction (right, black) rate ($nmol mol^{-1} h^{-1}$). From left to right the background is shaded blue for the UVC, peach for the UVB, and gray for the UVA regions of the electromagnetic spectrum. Blue vertical dashed lines show where the product and destruction curves intersect the primary emission wavelengths from GUV222 (left, 222 nm) and GUV254 (right, 254 nm).

At 222 nm the O_3 production rate is approximately two orders of magnitude greater than the rate of O_3 destruction. At 222 nm O_3 is not photolyzed rapidly enough to generate appreciable

OH. Thus, the major indoor air oxidant associated with GUV222 is O_3 . After 222 nm the O_2 cross section decreases rapidly such that at 254 nm no O_3 is produced from O_2 photolysis. The O_3 cross section peaks at 254 nm and thus photolysis of O_3 is important. While most of the O_3 will photolyze and immediately re-form O_3 , a small fraction on the order of 5 % to 20 %, depending on relative humidity, will form OH radicals.

When formed, O_3 will mostly react with chemicals in the air or on surfaces that contain carbon-carbon double bonds. OH, on the other hand, will react predominately in the gas phase with most gases in the air. The resulting chemistry from both oxidants can generate byproducts potentially degrading indoor air quality.

In the following sections we present measurements of GUV spectral irradiance and impacts on air quality in laboratory tests and a real indoor space.

2. Characterization of GUV Spectral Irradiance

2.1. Test Design: Spatial Spectral Irradiance Measurements

To characterize the spectral irradiance emitted by the GUV devices, we calibrated a commercial spectrometer measuring over a spectral range of 200 nm to 415 nm with a small integrating sphere attached via a fiber optic patch cable. The spectral range was wavelength-calibrated using Mercury-Argon, Krypton, and Neon reference pen lights with known emission peaks at 253.65 nm, 296.73 nm, 336.99 nm, 363.37 nm, and 377.34 nm. The spectral irradiance measurements were calibrated using both a NIST calibrated FEL lamp and a NIST calibrated Deuterium (D) lamp. The FEL lamp calibrations typically go down to a minimum wavelength of 250 nm; therefore, the D lamp is needed to extend the calibration regime down to about 200 nm. The bounded irradiance measurements have an uncertainty of 3.57 % ($k = 2$).

The integrating sphere was mounted onto a robotic arm with a custom adapter as shown in Figure 2. Before beginning measurements, the lamp was given 15 minutes to stabilize. Then the robotic arm was swept through the X-Z plane (horizontal-vertical plane) relative to the lamp source while being kept at a fixed distance from the front face of each source. Measurements were taken at 0 cm, 1 cm, 5 cm, 10 cm, 20 cm, 50 cm, and 100 cm from the front of the lamps. The spacing of measurements was adjusted depending on the distance from the lamp as shown in Table 1. Bounded irradiance measurements were taken from 250 nm to 257 nm for the GUV254 lamp to capture the relevant irradiance impacting GUV254 chemistry. The GUV222 lamp irradiance values were calculated by numerical integration from 205 nm to 235 nm due to its broader emission peak.

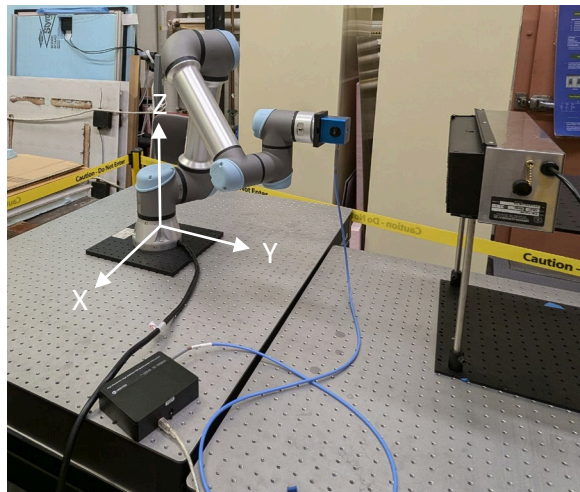


Figure 2. Robotic arm with integrating sphere and calibrated spectrometer assembly set up to measure spectral irradiance from GUV254 lamp. Set up was similar for GUV222 lamp. Coordinate system for the robot is shown.

Table 1 Horizontal and Vertical Increments for Spatial Lamp Irradiance Measurements. Increments were optimized for the expected irradiance distribution from each lamp. The GUV254 lamp uses a reflector to minimize the irradiance spread in the Z-direction.

Distance from Lamp (cm)	GUV254		GUV222	
	Horizontal (X) Increment (cm)	Vertical (Z) Increment (cm)	Horizontal (X) Increment (cm)	Vertical (Z) Increment (cm)
0	0.5	0.5	0.5	0.5
1	2	1	0.5	1
5	2	2	2	1
10	2	1	2	2
20	2	1	2	2
50	3	1	5	2
100	5	1	5	5

2.2. GUV254 Lamp Emission

The GUV254 lamp measurements are shown in Figure 3 and Figure A.1 (the same data but each plot uses the same color bar scale to demonstrate variations with distance). The front face of the lamp is 10 cm tall and 50 cm wide. The maximum irradiance was measured at the center of the lamp and was 16.5 W m^{-2} . The lamp irradiance falls off slowly relative to an inverse square law as the distance from the lamp increases. At 100 cm from the lamp's center, the peak measurement was 1.07 W m^{-2} . Notably, the vertical projection does not widen dramatically at 100 cm, only broadening from about 10 cm tall to 20 cm tall. This effect is likely due to the parabolic reflector within the lamp casing.

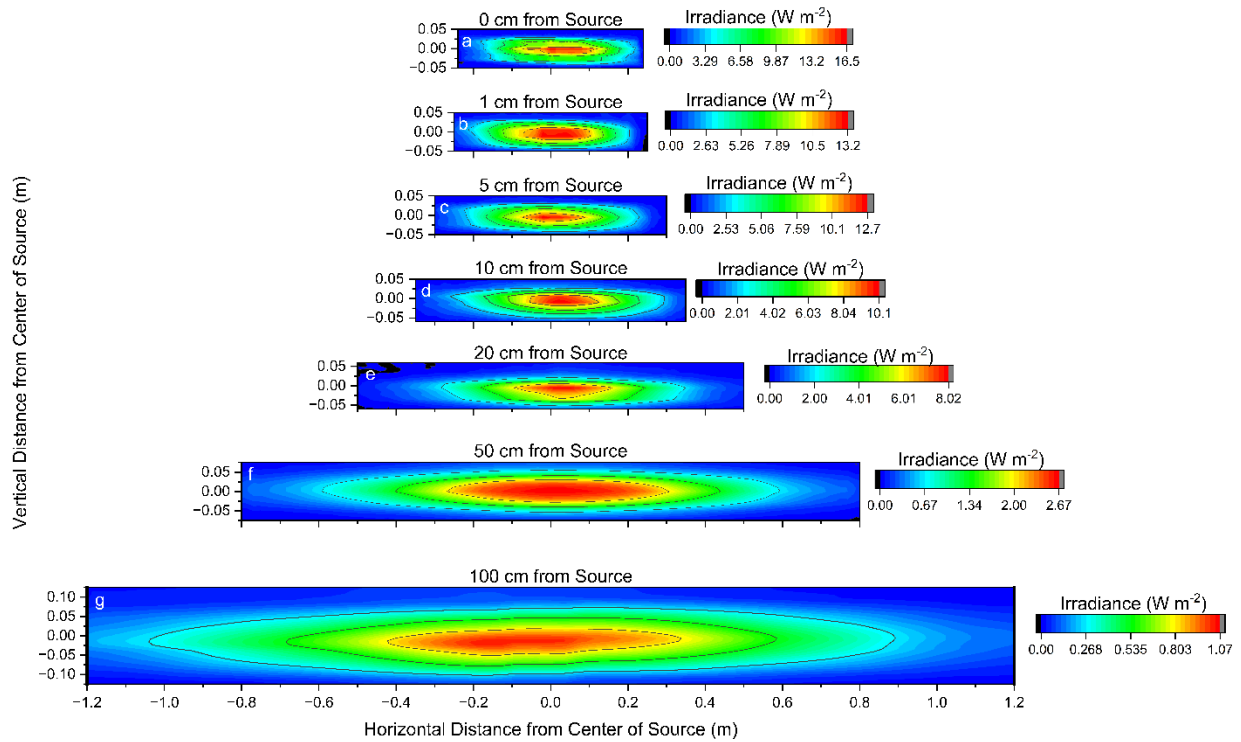


Figure 3. Bounded irradiance of 254 nm lamp measured in planes of a) 0 cm, b) 1 cm, c) 5 cm, d) 10 cm, e) 20 cm, f) 50 cm, and g) 100 cm from source. Irradiance values are integrated over 250 nm to 257 nm to capture emission at 254 nm. Irradiance color bar is unique for each distance. To visualize irradiance decay over distance with a constant irradiance color bar see Figure A.1.

2.3. GUV222 Lamp Emission

The GUV222 lamp has a much broader dispersion and acts more like a point source when moving further from the lamp as seen in Figure 4 and Figure A.2 (the same data but each plot use the same color bar scale to demonstrate variations with distance). The lamp opening is only 4 cm by 5 cm. An interesting characteristic of the lamp is the protrusion that forms on top of the emission region from 10 cm out to 50 cm. The emission generally becomes circular as it projects beyond 50 cm. The irradiance also falls off much more rapidly from 125.5 W m^{-2} to 0.230 W m^{-2} over 100 cm. Compared to the 254 nm lamp, this 222 nm lamp more closely follows an inverse square law decay as discussed in Link, et al. [22].

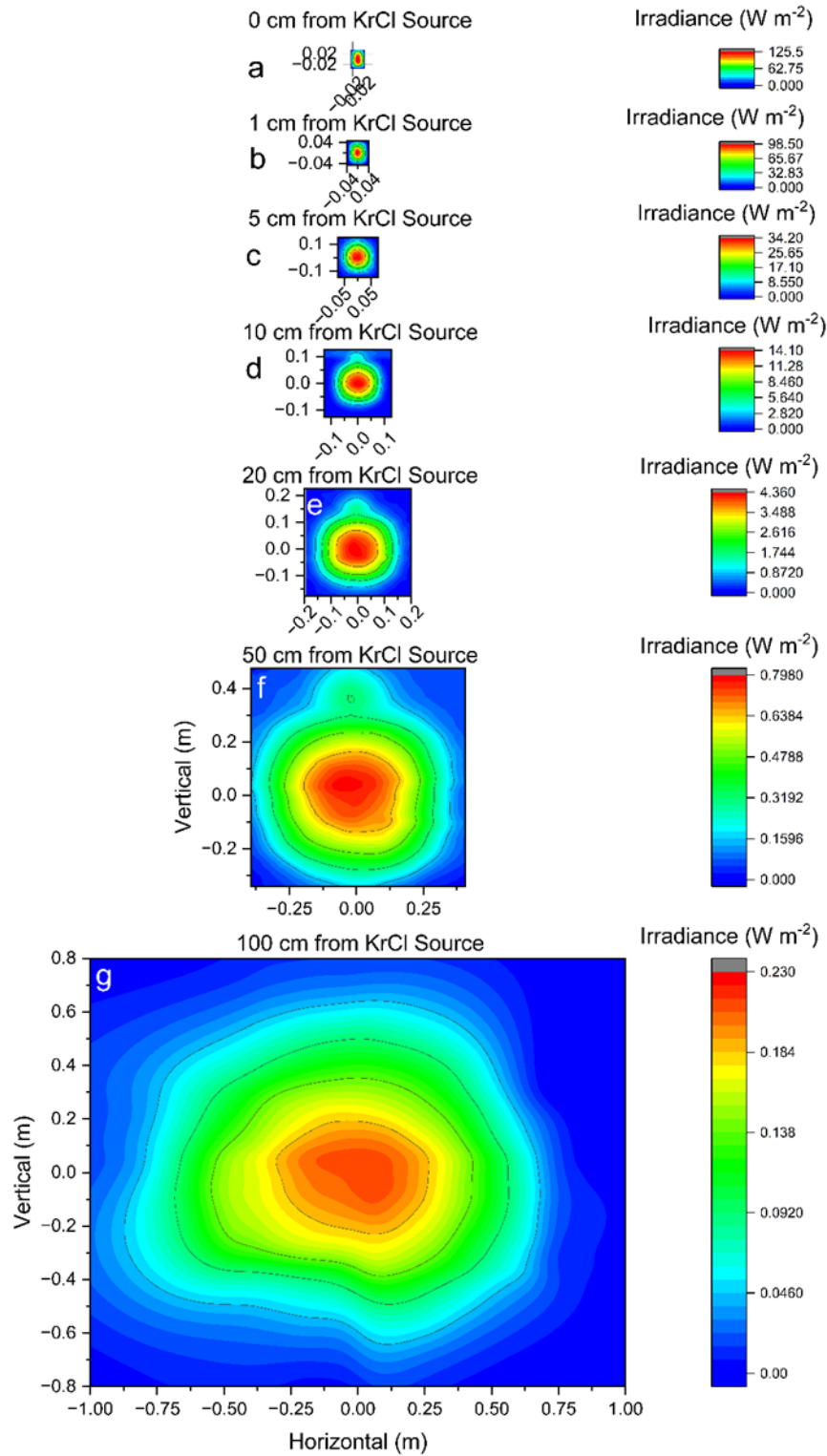


Figure 4. Bounded Irradiance from KrCl 222 nm source measured in planes of a) 0 cm, b) 1 cm, c) 5 cm, d) 10 cm, e) 20 cm, f) 50 cm, and g) 100 cm from source. Irradiance values are integrated over 205 nm to 235 nm which gives the total emission of the lamp. Irradiance color bar is unique for each distance. To visualize irradiance decay over distance with a constant irradiance color bar see Figure A.2.

3. Air Quality Impacts from GUV Operation in Laboratory Tests

3.1. Laboratory Test Design: ASTM Method WK81750

The GUV254 and GUV222 devices described in Section 2 were tested to characterize and quantify air byproduct formation following proposed ASTM standard test method WK81750 “The Chemical Assessment of Air Cleaning Technologies”. Details of the experimental methods can be found in Link, et al. [18], but will be briefly summarized here. A 31.5 m³ stainless-steel, temperature and humidity-controlled chamber was used to measure VOC and particle removal efficiency and potential for byproduct formation for portable air cleaners (Figure 5). A single GUV222 device and single GUV254 device were tested.

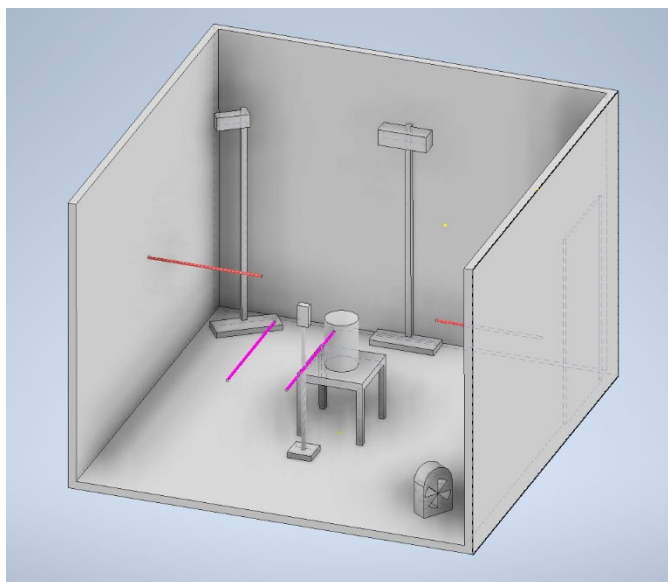


Figure 5. The 31.5 m³ environmentally controlled chamber used for quantifying air byproduct formation from GUV devices. Red lines indicate VOC (left) and particle (right) sampling lines. Pink lines shown chemical (left) and particle (right) injection lines. The GUV222 device is shown pointed down towards the center of the room on the left and the GUV254 device is shown illuminating the upper part of the space on the right.

The ASTM standard method consists of four tests. Two tests focus on measuring particle removal. Since the GUV devices did not remove particles, these tests are not discussed here. The other two tests discussed here focused on VOC and O₃ removal and/or air byproduct formation.

To perform the two tests the chamber was first controlled to 20 °C and 50 % relative humidity and then sealed. When the chamber was sealed no forced air ventilation or air recirculation was active. A mixing fan in the chamber was on during the test. After sealing the chamber, five chemicals, representing the challenge chemical suite, were injected into the chamber: formaldehyde (HCHO), decamethylpentacyclosiloxane (D5), limonene, o-xylene, and tetrachloroethylene (PERC). Different gas-phase concentrations of challenge chemicals were achieved in the chamber (20 nmol mol⁻¹ HCHO, 1 nmol mol⁻¹ D5, 5 nmol mol⁻¹ limonene, 3 nmol mol⁻¹ o-xylene, 2 nmol mol⁻¹ PERC). O₃ was also injected to achieve an initial 10 nmol mol⁻¹

concentration. These concentrations were intended to be similar to concentrations reported from surveys of concentrations in residential and commercial buildings. Chemical concentrations were measured using proton-transfer reaction mass spectrometry for all VOCs reported herein except for HCHO which was measured using infrared absorbance spectrometry.

Immediately after injection of the chemical suite (including O₃) Test 1 was started and chemical concentrations decayed in the chamber over four hours due to leakage of air into the chamber (called here “natural decay”) and reactions. Figure 6 shows an example of the natural decays of the challenge chemical suite observed for Test 1 (GUV device off). The first-order loss constant (k_{decay}) for each chemical was determined by performing a linear fit of the natural log of the chemical concentration as a function of time divided by the initial chemical concentration.

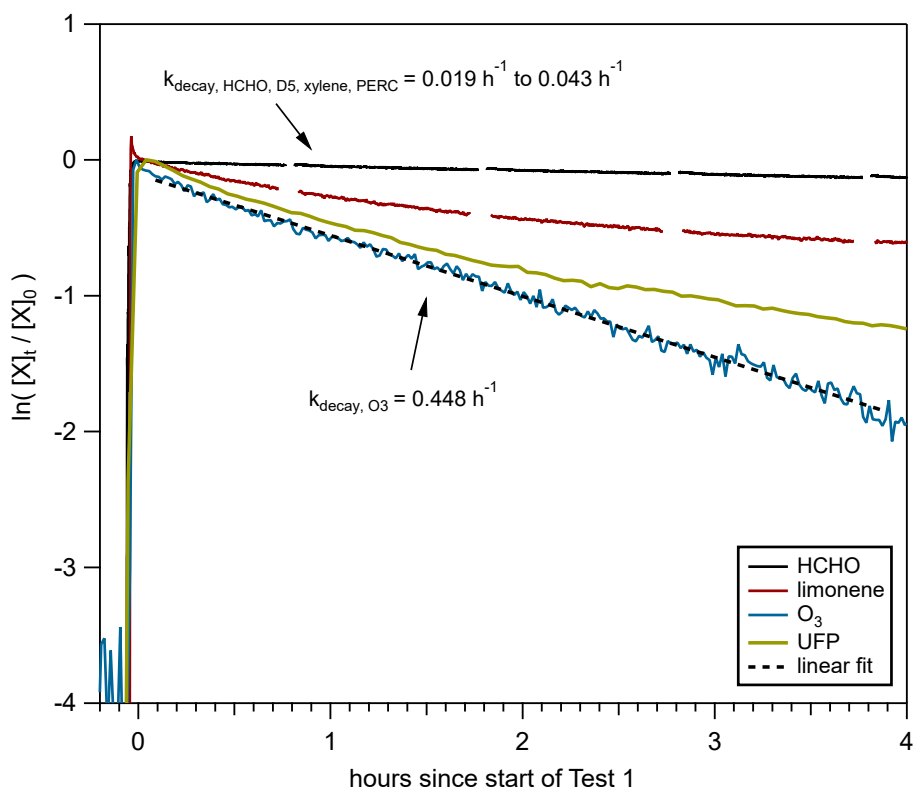


Figure 6. Concentration decay of select challenge chemicals observed during Test 1. $[X]$ is the concentration of a challenge chemical. k_{decay} is the slope of a linear fit of the natural log of the chemical concentration as a function of time divided by the initial chemical concentration compared to time. The concentration data and fits for all chemicals other than limonene, O₃, and ultrafine particle (UFP) are indistinguishable from each other at this scale and represented by the black HCHO line. Note: Uncertainty in k_{decay} was less than 6 % for any given linear fit determination whereas variability of k_{decay} between replicate tests was within 20 %.

Test 2 was performed with the same steps as Test 1, but at the start of the test the GUV device was turned on. Following the same calculation as presented for Test 1 we calculated a k_{decay} for each chemical in Test 2. If the k_{decay} for Test 2 was statistically larger than that of Test 1 we could calculate a clean air delivery rate from the difference in the decay constants. GUV222 only had measurable clean air delivery rates for limonene and PERC and no clean air delivery

rates were quantified for GUV254. Thus, we do not present any clean air delivery rate data here. By comparing the observations from Test 2 to Test 1 we could also quantify air chemistry byproduct formation. For our tests we define air chemistry byproducts from GUV as VOCs measured by the Proton-Transfer Reaction Mass Spectrometer (PTR-MS), HCHO, particulate matter, and O₃. Below we present observations of air chemistry byproduct formation from the two GUV technologies.

3.2. Byproduct Formation from GUV Under Test Conditions

3.2.1. O₃ Generation from GUV254

As expected, there was no measured O₃ generation from GUV254 in the laboratory test.

3.2.2. O₃ Generation from GUV222

We measured O₃ generation from GUV222 in the laboratory test (Figure 7).

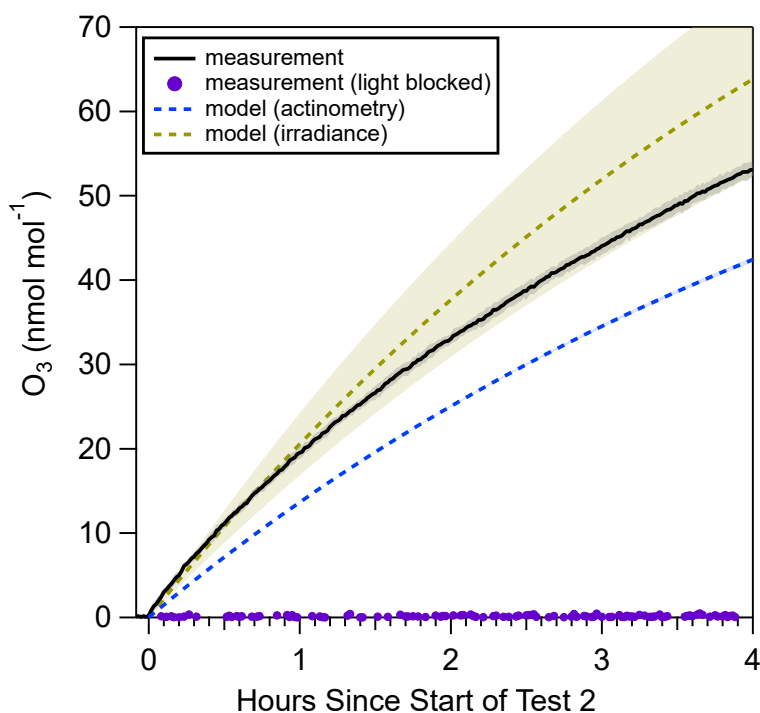


Figure 7. O₃ generated from GUV222 measured (black solid line) during seven replicates of Test 2. Two model predictions of O₃ generation are shown where the fluence rate was estimated from spectral irradiance measurements (yellow dashed line) and using PERC as an actinometer (blue dashed). Purple dots show that O₃ was not generated when the light output was covered.

O₃ reached maximum concentrations of 52 nmol mol⁻¹ ± 1 nmol mol⁻¹ (standard deviation of the average of seven replicate measurements) at the end of the four-hour tests. We covered the light output of the lamp for one test and did not measure any O₃ generation. This test confirmed that the O₃ was being generated from the 222 nm light and not from electrical

discharge in the device. We note that because the chamber was sealed the O₃ loss rate (e.g., approximately 0.2 h⁻¹) was lower than would be expected in real indoor environments and thus the O₃ concentrations measured in the chamber do not reflect the concentrations that would be expected to be observed in a real indoor space. Additional details of the O₃ generation measurements are presented in Link, et al. [22].

Figure 7 also shows two calculated O₃ concentration traces using O₃ production kinetics presented in Equation 3 and a GUV222 fluence rate estimated from two different methods. The measured O₃ concentration can also be used to back calculate a GUV222 fluence rate using Equation 3.

3.2.2.1. Estimating the GUV222 Fluence Rate Using Three Different Methods

Accurate determination of the room-averaged fluence rate from GUV222 is necessary to predict O₃ formation in indoor spaces. However, GUV222 fluence rates are hard to directly measure. We used three different methods to estimate the GUV222 room-averaged fluence rate (Table 2): (1) chemical actinometry using the photolytic loss of PERC, (2) projection and interpolation of the measured GUV222 irradiance field across the volume of the chamber, and (3) measured O₃ production.

Chemical actinometry (“Actinometry”) has been used in laboratory studies of chemical kinetics for decades. Often fluence is difficult to measure and instead a chemical tracer can be used to estimate the average fluence rate. We used the photolytic loss of tetrachloroethylene (PERC, C₂Cl₄) to determine the chamber averaged fluence rate (F, μW cm⁻²) following Equations 4 and 5, with the parameters the same as defined in Equations 1 and 2.

$$\frac{d[C_2Cl_4]}{dt} = -j_{C_2Cl_4}[C_2Cl_4] \quad (4)$$

$$j_{C_2Cl_4} = \int \sigma_{C_2Cl_4} \Phi_{C_2Cl_4} F d\lambda \quad (5)$$

Using this method we calculated a room-averaged fluence rate for the GUV222 lamp of 2.1 μW cm⁻² ± 0.1 μW cm⁻² (standard deviation of the average of five replicate measurements). The actinometry derived fluence rate can be used with equation (2) to model the ozone production from the GUV222 device (Actinometry in Figure 7).

As discussed in Section 2 we measured the radial and angular distribution of irradiance from GUV222. From these measurements we interpolated between available measurements in the geometric space and projected it in a 31.5 m³ volume representative of the chamber (method “Irradiance”). We then averaged over the volume to get an estimate fluence rate of 3.2 μW cm⁻² ± 0.3 μW cm⁻² (uncertainty propagated from standard deviation of replicate O₃ generation measurements). The irradiance derived fluence rate can be used with equation (2) to model the ozone production from the GUV222 device (Irradiance in Figure 7).

The final method we used to estimate the fluence rate (method “O₃ Production”) was by modeling the measured O₃ production. From Equation 3 the only variable that is unknown in the O₃ production equation is the photon flux (i.e., the fluence rate) and thus by minimizing the difference between modeled and measured O₃, with the fluence rate as the free variable, we

estimated a room-averaged fluence rate of $2.6 \mu\text{W cm}^{-2} \pm 0.1 \mu\text{W cm}^{-2}$ (standard deviation of the fluence rate average from seven model fits).

Table 1 summarizes the room-averaged fluence rates determined from the three different methods used in our study. Further details of how the measurements supporting the results from application of these three methods can be found in Link, et al. [18].

Table 2. Room-averaged fluence rates determined from three different methods.

Method	Room-averaged Fluence Rate
Actinometry	$2.1 \mu\text{W cm}^{-2} \pm 0.1 \mu\text{W cm}^{-2}$
Irradiance	$3.2 \mu\text{W cm}^{-2} \pm 0.3 \mu\text{W cm}^{-2}$
O ₃ Production	$2.6 \mu\text{W cm}^{-2} \pm 0.1 \mu\text{W cm}^{-2}$

3.2.3. VOC Byproduct Formation from GUV254 and GUV222

We observed VOC byproduct formation from both GUV254 and GUV222 in the chamber tests. Figure 8 shows background subtracted speciated VOC concentrations measured during Test 2.

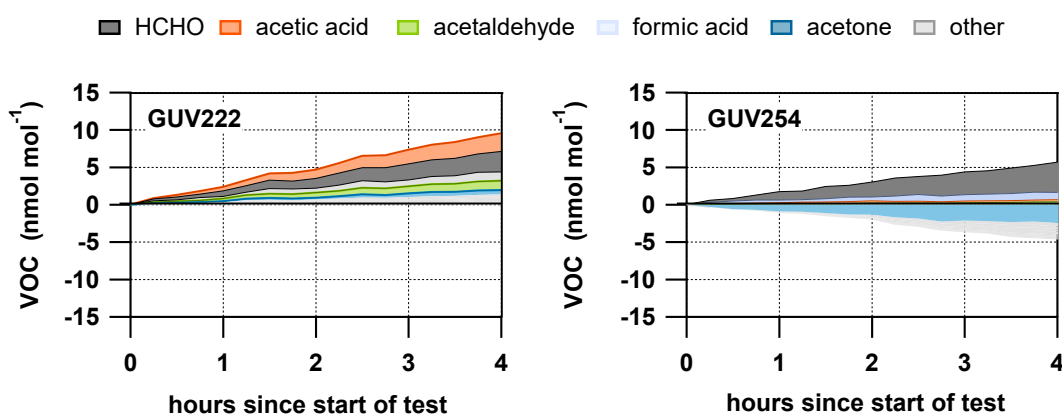


Figure 8. Speciated VOC concentrations measured during Test 2 for GUV222 and GUV254.

Increases in HCHO were observed from both GUV technologies and increases in acetaldehyde were observed for GUV222. An increase of approximately 2 nmol mol^{-1} of VOCs that included saturated aldehydes, ketones, and assumed limonene oxidation products was also observed for GUV222. Decreases of approximately 5 nmol mol^{-1} of non-HCHO VOCs were measured for the GUV254 technology among which acetone constituted more than half of the total decrease. The acetone absorption cross section peaks at 254 nm and thus the loss of acetone is likely associated with photolysis.

Figure 9 shows the net change in VOC concentration when the VOC concentration generated is added to the VOC concentration decrease observed in Test 2.

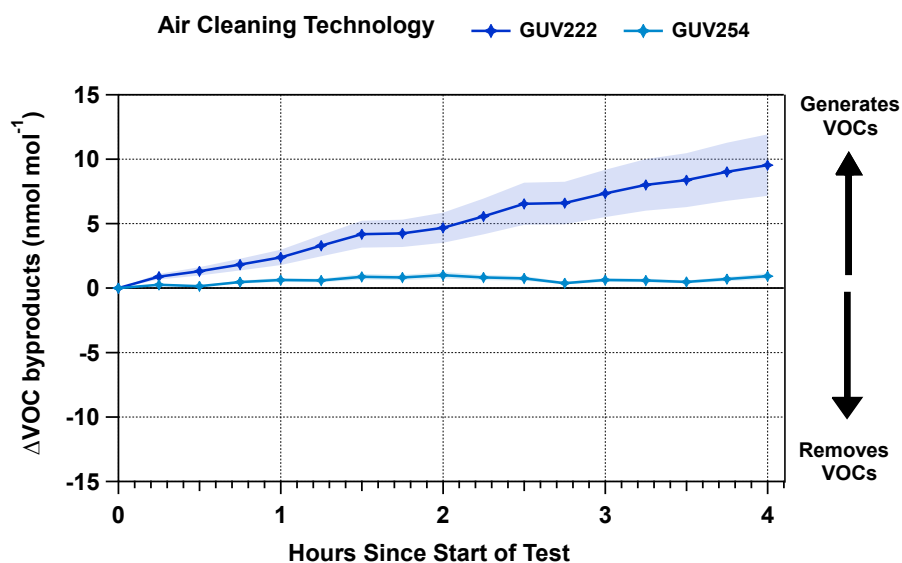


Figure 9. Net VOC concentration change during Test 2 for GUV222 and GUV254. Uncertainty for GUV222 is shown via shaded region. Uncertainty ($\pm 25\%$ from propagation of calibration uncertainties) for GUV254 is not visible at this scale.

From the perspective of net VOC concentration change, VOC concentrations increased by roughly 10 nmol mol^{-1} over the course of Test 2 for GUV222 while concentrations did not change significantly for GUV254. As shown in Figure 8 simultaneous generation and removal of VOCs is occurring resulting in a net zero change in total VOC concentrations for GUV254. In contrast, GUV222 was observed to only generate VOCs. We suspect VOC removal observed from GUV254 was from some combination of photolysis by 254 nm light and some production of OH radicals. OH is less discriminate of a gas-phase oxidant than O_3 and will react with many VOCs whereas O_3 only reacts at rates comparable to OH with select unsaturated VOCs (e.g., limonene).

3.2.4. Particulate Matter Formation

For the tests we focused on measurements of ultrafine particulate matter (i.e., particles with a diameter less than 100 nm) formation from GUV. Ultrafine particles were formed from both technologies during Test 2 with GUV222 forming more particulate matter by both number and volume than GUV254 (Figure 10).

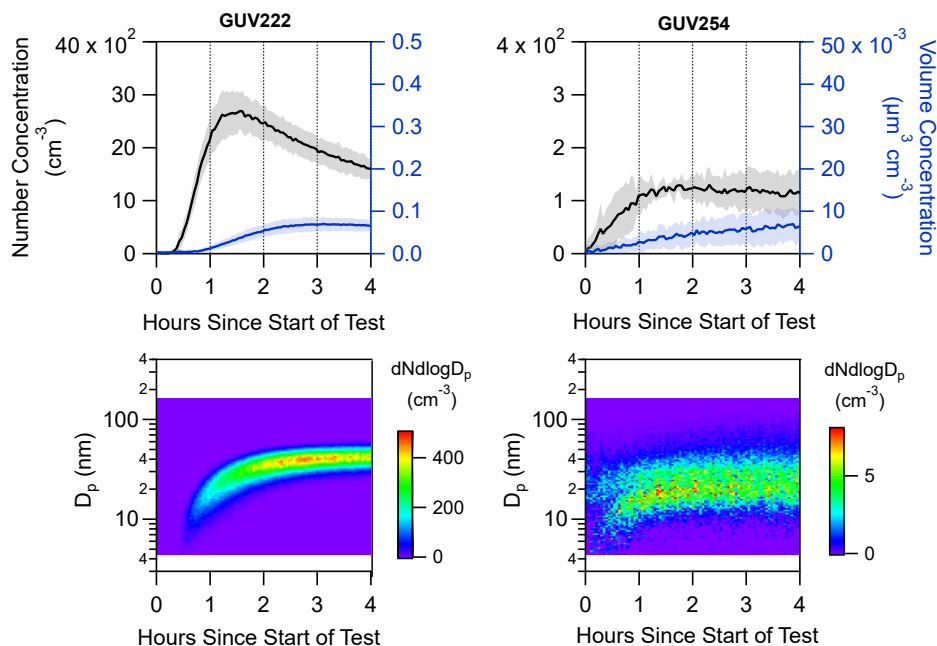


Figure 10. Ultrafine particle production from GUV222 and GUV254. Top panels show total number concentrations. Bottom panels show the particle diameter specific concentrations. Each panel has a different scale.

GUV254 generated an order of magnitude fewer particles than GUV222. Particle generation was driven by nucleation of oxidized vapors reflected by increases in particle number concentrations at small diameters that then grow in size through condensation and coagulation. Assuming a particle density of 1 g cm^{-3} and converting particle volume concentration to mass concentration both technologies produced less than $0.1 \mu\text{g m}^{-3}$ of aerosol. As discussed in the supplement of Link, et al. [18], this may be an underestimate of potential aerosol mass formation because background aerosol in real indoor spaces serve as condensation sinks for condensable vapors. Increased condensation sites for condensable vapors can potentiate aerosol mass formation that only occurred through nucleation in our chamber experiment.

3.2.5. Evidence for VOC Photolysis from GUV254 and GUV222

We focus our analysis of the effects of GUV on indoor air chemistry on the generation of gas-phase oxidants because that chemistry is relatively well-understood. Less understood is the possible influence of gas-phase or surface photolysis of VOCs from GUV. Above (Figure 8) we showed that GUV254 caused decreases in acetone concentrations that were likely associated with acetone photolysis from absorption of 254 nm light. Photolysis of acetone, and other ketones, results in the formation of organic radicals [26] that can oxidize VOCs, generate OH radicals, and/or form secondary organic aerosol. We likely observed VOC photolysis from GUV254 in the chamber, but real-world studies are needed to determine if this process may be important in real indoor spaces.

For GUV222 we successfully employed PERC (C_2Cl_4) as an actinometer because of its propensity to photolyze from irradiation with 222 nm light as described in Sec. 3.2.2.1. Peng, et al. [31] used another VOC, tetrabromomethane (CBr_4), as an actinometer to measure the fluence rate from GUV222 following the same method described in this study. Use of these two VOCs as actinometers demonstrates that GUV222 has the potential to photolyze VOCs containing halogen moieties and thus may induce chemistry through photolysis indoors when cleaning is occurring, for example. In addition to possible photolysis of organohalogens, Deal, et al. [30] recently demonstrated efficient photolysis of gas-phase lactic acid from 222 nm light. Further laboratory and field studies characterizing VOC photolysis from GUV222 are warranted.

4. Air Quality Impacts from GUV Operation in a Restroom

We used a public restroom in a building on the NIST campus as a case study to investigate the potential of GUV installed in a real indoor space to generate unintended air byproducts. We chose a restroom for this investigation because application of GUV is suggested to have the greatest benefit in public spaces where occupants may be in close contact and behavioral airborne virus transmission mitigation strategies (e.g., mask wearing) are not exclusively relied upon for infectious disease control. When exploring options for GUV case studies we found the forced air ventilation system to the restroom was broken. This feature of the restroom also highlighted a common problem encountered in many commercial buildings; ventilation systems are often poorly maintained or unknowingly dysfunctional. Current discussions of GUV standardization, GUV222 in particular, often assume the technology will be installed in buildings with working ventilation systems. From an air quality perspective, a major problem with this assumption is that when ventilation rates decrease, steady-state concentrations of VOCs (emitted from various indoor sources and infiltrated from outdoor air) increase, and concentrations of unintended air byproducts from GUV-oxidation chemistry may increase. Below we outline the methodology, results, and conclusions from our real-world installations of GUV222 and GUV254 in a restroom. This work is discussed in greater detail in Link, et al. (2024) [32].

4.1. Restroom Installation Experiment Design

The restroom used for GUV installations and testing is 59 m³ (Figure 11). Gas sampling lines were run from a nearby conference room, where instrumentation was located, to the restroom to sample VOCs, O₃, and nitrogen oxides (NO + NO₂ = NO_x).

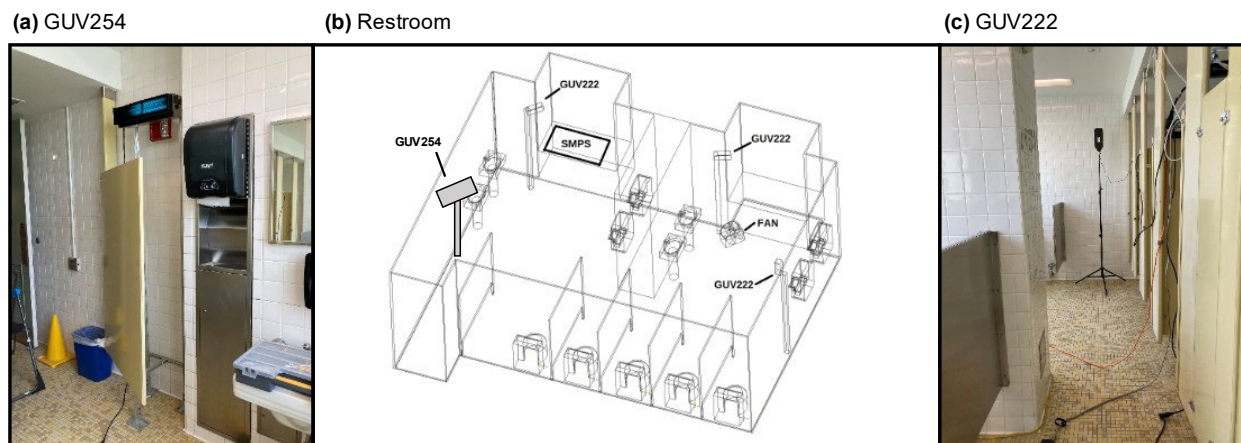


Figure 11. (a) Picture of GUV254 installation in restroom. (b) Diagram of restroom GUV installations and experiment. (c) Picture of GUV222 installation in restroom.

A scanning mobility particle sizer (SMPS) was located in the restroom to measure particle size distributions. Three GUV222 lamps were installed at various locations in a configuration to optimize direct irradiation of potential occupants. Using ozone generated from GUV222 as an actinometer we estimate the room-averaged fluence rate to be $3.2 \mu\text{W cm}^{-2} \pm 0.6 \mu\text{W cm}^{-2}$. A

single GUV254 lamp was installed towards the entrance of the restroom and positioned so it irradiated the longest part of the restroom. A mixing fan was installed in the restroom and turned on periodically to measure the influence of air mixing on byproduct formation from GUV.

Measurements of air byproduct formation during GUV operation were conducted over two weekends. No one entered the restroom either weekend. The first weekend (Wk1) was characterized by a lower air change rate of roughly 1 h^{-1} , as measured by sulfur hexafluoride (SF_6) tracer pulse injection decay. As part of normal operations custodial staff installed fragrant screens in the urinals that served as an emission source of reactive gas-phase VOC precursors for oxidation chemistry days before Wk1 experiments. Facilities staff fixed the broken forced air ventilation system before the start of weekend 2 (Wk2) which increased the air change rate to 2 h^{-1} . VOC concentrations were about five times higher in the restroom for weekend 1 (Wk1) compared to weekend 2 (Wk2). GUV222 lamps were run for three hours on then three hours off cycles in Wk1 and four hours on then four hours off cycles in Wk2. GUV254 was operated for three hours on then three hours off cycles in Wk1 and not operated in Wk2.

4.2. GUV254 in the Restroom

No ozone, formaldehyde, VOC oxidation products or ultrafine particle byproduct generation was discernable from background variability due to operation of GUV254 in the restroom on Wk1 (Figure 12). Because no byproducts were observed under conditions of lower air change rate and higher oxidation chemistry precursor concentrations, we did not operate GUV254 on Wk2 when conditions were less favorable for byproduct formation from oxidation chemistry (lower VOC concentrations). GUV254 generated less air chemistry byproducts in the chamber compared to GUV222 so the lack of measurable air chemistry byproduct formation in the restroom was expected. The modeling of Peng, et al. (2022) [19] also predicted less byproduct formation from GUV254 compared to GUV222.

4.3. Air Quality Impacts from GUV222 in the Restroom

Several air byproducts were generated from operation of GUV222 in the restroom both weekends. We highlight the formation of four key air byproducts:

- (1) O_3
- (2) $\text{VOC}_{\text{O}_3 \text{ Ox}}$: the sum of 34 VOCs observed to increase in concentration when GUV222 was turned on
- (3) Ultrafine Particulate Matter (Particle Number): quantified as in units of 10^3 cm^{-3}
- (4) Ultrafine Particulate Matter (Aerosol Mass): quantified in units of $\mu\text{g m}^{-3}$

4.3.1. Generation of O_3 , VOC Oxidation Products from O_3 Chemistry, and Particulate Matter

Figure 12 shows time series of the four key air byproducts and the variability of their formation when the GUV222 and GUV254 lamps were off versus when they were on in Wk1..

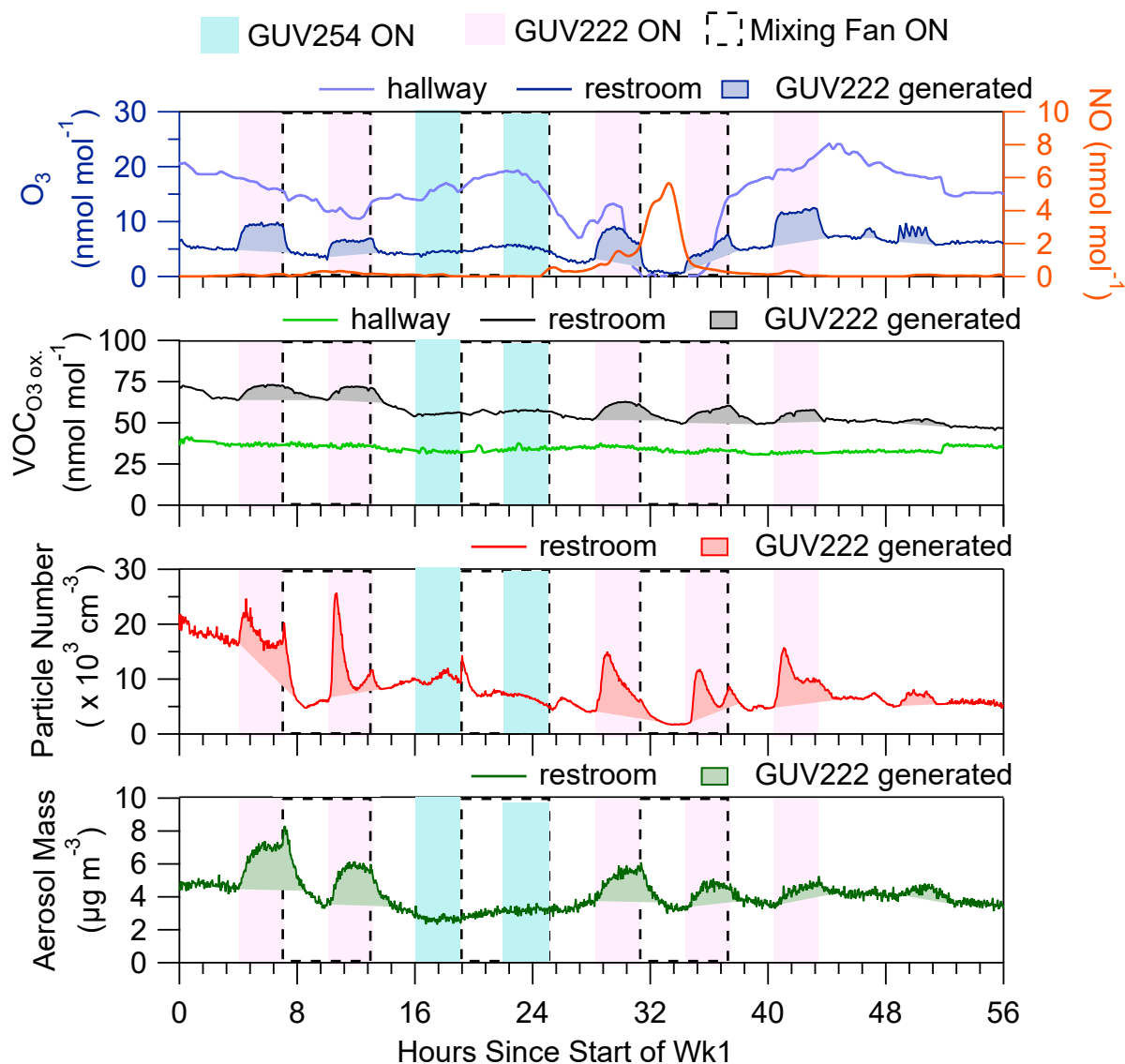


Figure 12. The air change rate in Wk1 was about 1 h^{-1} . Byproducts include O_3 (blue), $\text{VOC}_{\text{O}_3 \text{ ox}}$ (black), particle number (N_p , red), and particle mass (M_p , green) concentrations. Pink shaded regions show when GUV222 was on. Blue shaded regions show when GUV254 was on. Dotted lines indicate the 8-hour periods where a mixing fan was on. Shaded areas below the traces show the estimated increase in byproduct concentrations generated by GUV222. Hallway concentrations of $\text{VOC}_{\text{O}_3 \text{ ox}}$ and O_3 are used in O_3 and $\text{VOC}_{\text{O}_3 \text{ ox}}$ generation rate calculations. A decrease in O_3 concentrations (dark blue for restroom and light blue for hallway) with increased NO (orange) concentrations is shown. $\text{VOC}_{\text{O}_3 \text{ ox}}$ is the sum of 34 VOCs observed to increase in concentration when GUV222 was turned on. The y-axis for particle number is the particle number divided by 1000. The uncertainty in O_3 concentrations is $\pm 0.3 \text{ nmol mol}^{-1}$. The uncertainty in $\text{VOC}_{\text{O}_3 \text{ ox}}$ is $\pm 25 \%$. The uncertainty in particle number concentrations is $< 1 \%$, but the conversion of particle number concentrations to aerosol mass carries an uncertainty of 10% from the SOA density estimate.

Every time GUV222 is turned on O_3 is generated and increases concentrations above background on average by 5 nmol mol^{-1} . O_3 chemistry was enhanced above background resulting in the generation of oxidized VOCs originating from the O_3 chemistry ($\text{VOC}_{\text{O}_3 \text{ ox}}$) and

particulate matter. Spikes in particle number concentrations, after GUV222 was turned on, decreased over time due to coagulation of smaller particles that formed larger particles. Aerosol mass was also generated from GUV222 O₃ chemistry with maximum concentrations of 2.6 μg m⁻³ generated above background and 1.7 μg m⁻³ generated on average across the five on/off cycles.

Figure 13 shows that lower concentrations of byproducts (except O₃) were formed from operation of GUV222 during Wk2 when the air change rate was roughly 2 h⁻¹.

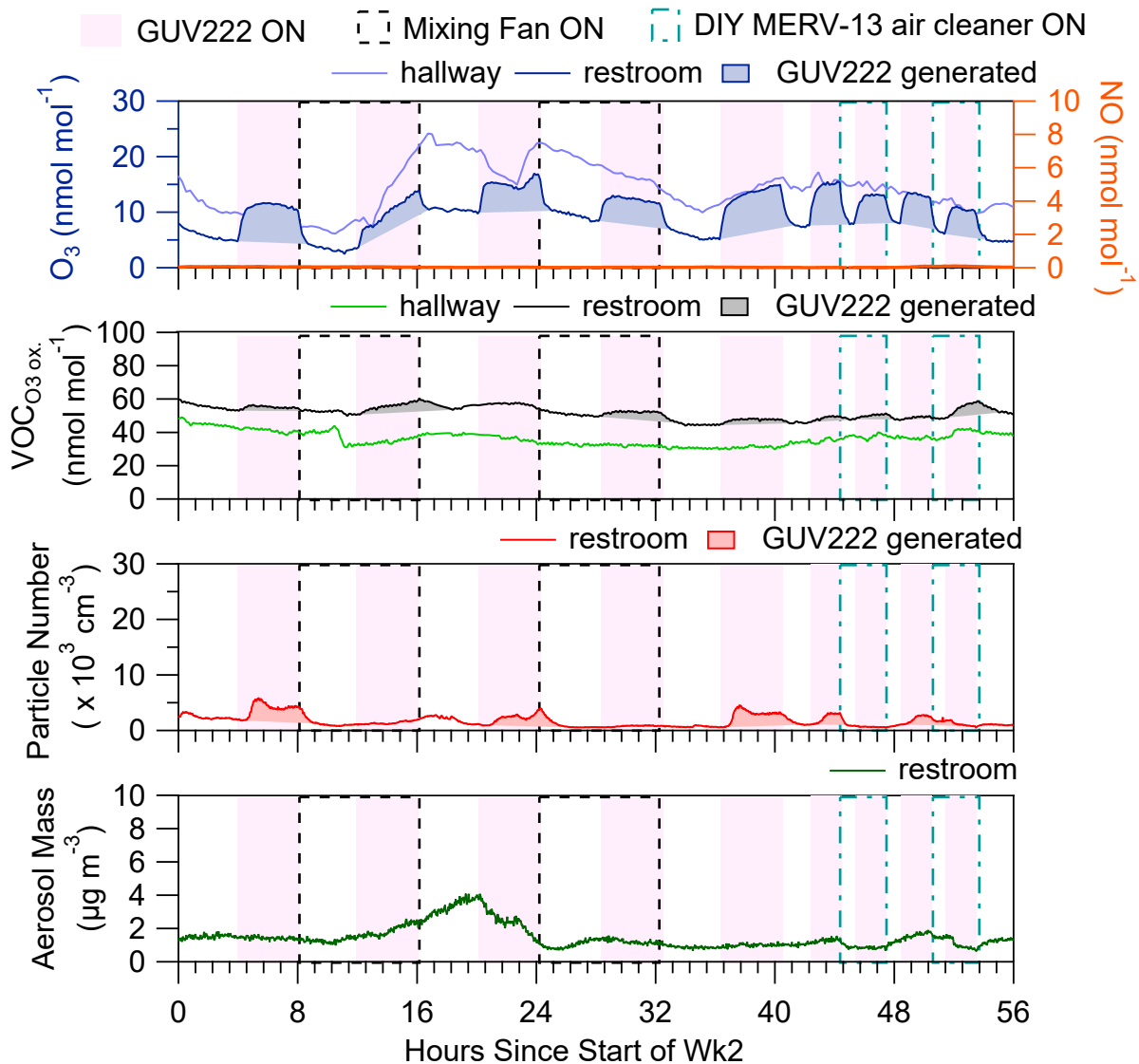


Figure 13. The ACR in Wk2 was about 2 h⁻¹. The descriptions in the caption for **Figure 12** apply to this figure also. A MERV-13 do-it-yourself (DIY) air cleaner was used for two GUV222 on/off cycles at the end of the weekend (teal dotted lines and dots).

Because of a combination of increased ventilation and lower VOC concentrations (due to a combination of decreased direct emissions and increased ventilation) lower concentrations of

VOC and particulate byproducts were formed from GUV222 O₃ chemistry. No aerosol mass was generated that was discernable above background. Lower amounts of ultrafine particles were generated, but when the DIY air cleaner was used particle formation was suppressed.

4.3.2. VOC Oxidation Products from O₃ Chemistry (VOC_{O₃ Ox.})

Thirty-four individual VOCs, identified as ions as measured by the PTR-MS (except HCHO which was measured with infrared spectrometry), increased in concentration during GUV222 operation. We define these VOCs as O₃ chemistry oxidation byproducts (VOC_{O₃ Ox.}). We classified VOC_{O₃ Ox.} into three broad categories: aldehydes, terpenoid oxidation products, and other VOC_{O₃ Ox.} (Figure 14).

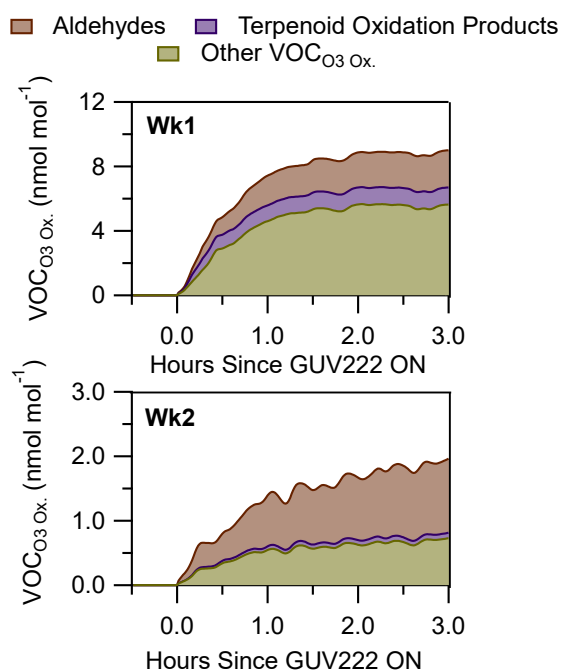


Figure 14. Average time series of VOC_{O₃ Ox.} produced from GUV222 during Wk1 and Wk2.

Aldehydes included C₁ through C₁₀ saturated aldehydes, acrolein, and methacrolein. HCHO made the largest contribution to the aldehyde group and is a VOC byproduct that has been linked to adverse health outcomes. Terpenoid oxidation products included VOCs with elemental formula corresponding to C₉ and C₁₀ compounds that likely originated from oxidation of terpenoid VOC precursors emitted from the urinal screens. We cannot differentiate structural isomers of terpenoid oxidation products with the PTR-MS measurement and consequently we do not have an understanding of possible effects on health from exposure. Other VOC_{O₃ Ox.} included compounds like acetone, acetic acid, and propanoic acid—VOCs that are not generally associated with adverse health effects.

4.3.3. Ultrafine Particle Generation

Ultrafine particles, defined here as particles with a diameter less than 100 nm, present a unique exposure risk compared to larger particles that mostly contribute to PM_{2.5} (defined in units of $\mu\text{g m}^{-3}$ and represents the integrated aerosol mass concentration of particles with diameters of 2.5 μm or less) because they can penetrate and potentially deposit to greater extent deep in the lungs where transfer into the bloodstream may occur. Ultrafine particle generation was observed both weekends with Wk1 having greater production than Wk2 (Figure 15).

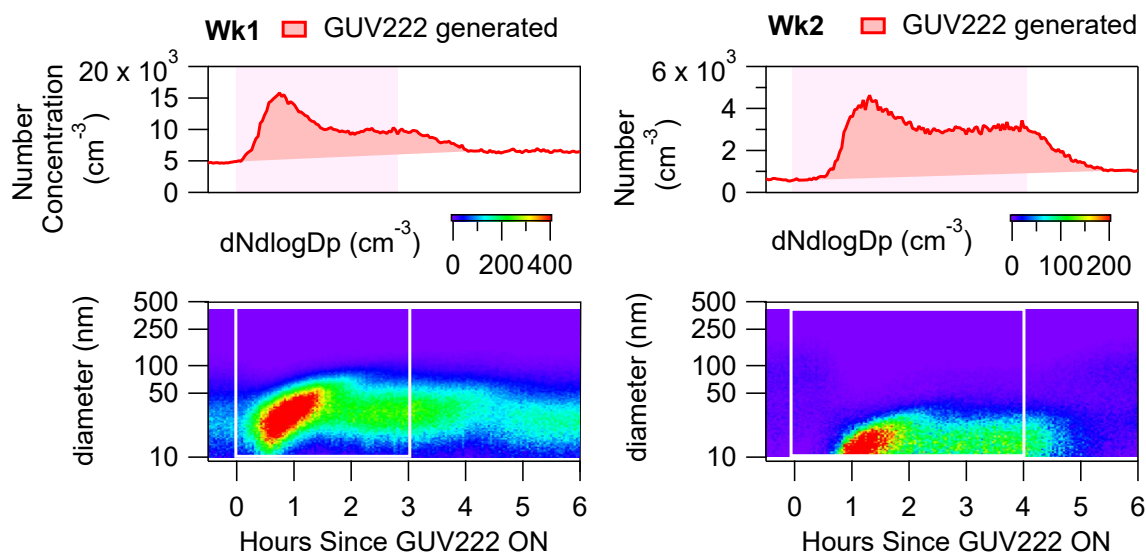


Figure 15. Ultrafine particle number concentrations (top, note different scales) for Wk1 (left) and Wk2 (right) with lognormal number size distributions (dN/dlogDp; bottom).

Ultrafine particles were generated during GUV222 operation from nucleation. As shown in Figure 15, when particle number concentrations peak most of those particles are in the very small sizes (< 30 nm) that originate from the nucleation of particles from condensable vapors. O₃ oxidation of terpenoids emitted from the urinal screens are assumed to drive the new particle formation events. Shortly after particle number concentrations peak, they decrease due to coagulation. This is reflected in the aggregation of particle number concentrations into increasingly larger particle sizes. These particle dynamics occur both weekends, but particle concentrations are distributed at smaller count median diameters in Wk2 compared to Wk1.

4.3.4. Aerosol Mass Generation

We measured the generation of aerosol mass, above background concentrations, from operation of GUV222 in Wk1. We assume the aerosol mass generated is secondary organic aerosol (SOA) largely formed from the O₃ oxidation of terpenoid precursors emitted from the urinal screens. Figure 16 demonstrates that we can explain, within 0.7 $\mu\text{g m}^{-3}$, the generation of SOA in the restroom from SOA yields of various terpenoid precursors measured in laboratory chamber studies, after accounting for wall loss of condensable vapors.

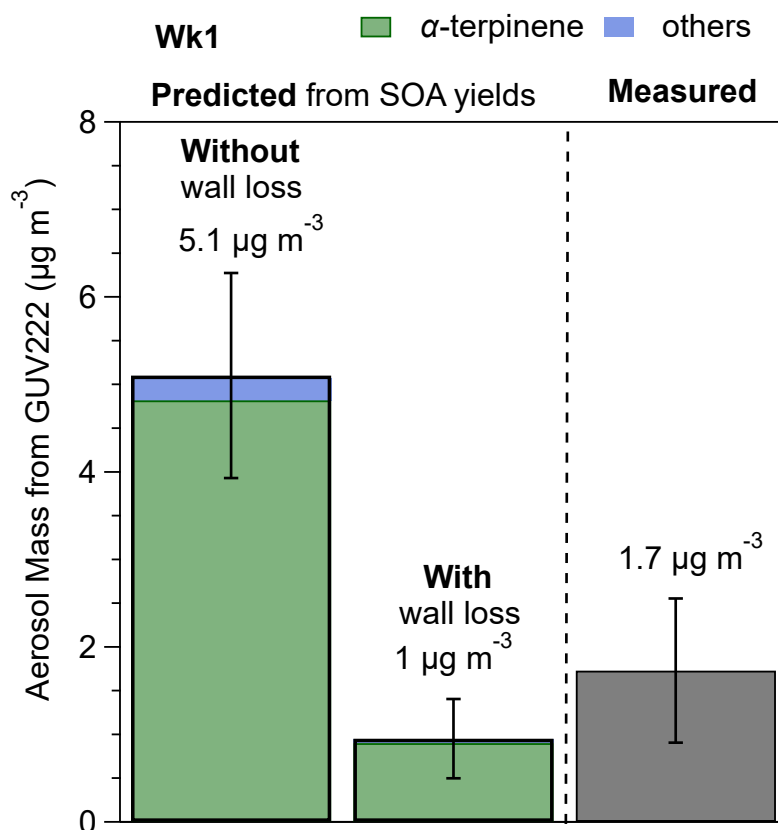


Figure 16. Aerosol mass production predicted from measurements of laboratory-determined secondary organic aerosol (SOA) yields compared to what was measured in Wk1. First two bars are predicted from reacted VOC concentrations and published SOA yields. The third bar is what was measured.

The condensable vapor wall loss parameterization and an extensive discussion of terpenoid precursor concentrations are presented in Link, et al. (2024) [31]. Two key observations arise from our analysis of vapor wall loss effects on SOA formation from O_3 chemistry with precursors in the restroom. (1) The amount of byproducts generated (SOA here) is dependent on the chemical loss of specific precursors. The O_3 oxidation of a single terpenoid precursor, α -terpinene, was likely responsible for most (> 95 %) of the SOA generated from GUV222 chemistry in the restroom. (2) The surface area to volume ratio of an indoor space is an important consideration when predicting the influence of O_3 + precursor chemistry on SOA formation. Approximately 10 % of the condensable vapors formed from terpenoid oxidation persisted in the gas-phase to potentially generate aerosol whereas the majority (> 60 %) was lost to condensation on walls and other surfaces.

5. Solar Influenced Irradiance Data

UV irradiation in and around the home can also play a role in air quality. Measuring the amount of incident solar irradiation throughout the year can help to better understand the magnitude of these impacts. To this end a commercial spectrometer assembled with a 3-way split fiber optic cable and three shutter-controlled integrating spheres was deployed inside the living room of NIST's Net-Zero Energy Residential Test Facility (NZERTF). The total bounded irradiance measured from this system has an uncertainty of 3.57 % ($k=2$). The assembly was calibrated in the same manner as the UV spectrometer-integrating sphere assembly from section 2.1 using the same FEL lamp. We found that the spectrometer was reliable in the region of 375 nm to 850 nm. One sphere was located at the eastern most south-facing window of the room, and another was located approximately 50 cm below a recessed ceiling light towards the northwestern (interior) region of the room.

5.1. Indoor Spatial and Temporal Total Irradiance

Error! Reference source not found. shows the bounded irradiance over the course of a day measured at the window (a) and towards the interior of the room (b). A sunny day near the spring equinox (3/21) and a sunny day near the summer solstice (6/22) were included. The roof overhang plays a significant role in allowing direct solar radiation to reach the window during the equinox, but not during the solstice. This design feature is meant to minimize cooling loads during the hot summer months and reduces the total sunlight exposed to the south facing windows. The measurements towards the interior of the house are not heavily influenced by the roof overhang as most of the light in this region is either diffuse sunlight or from the ceiling light.

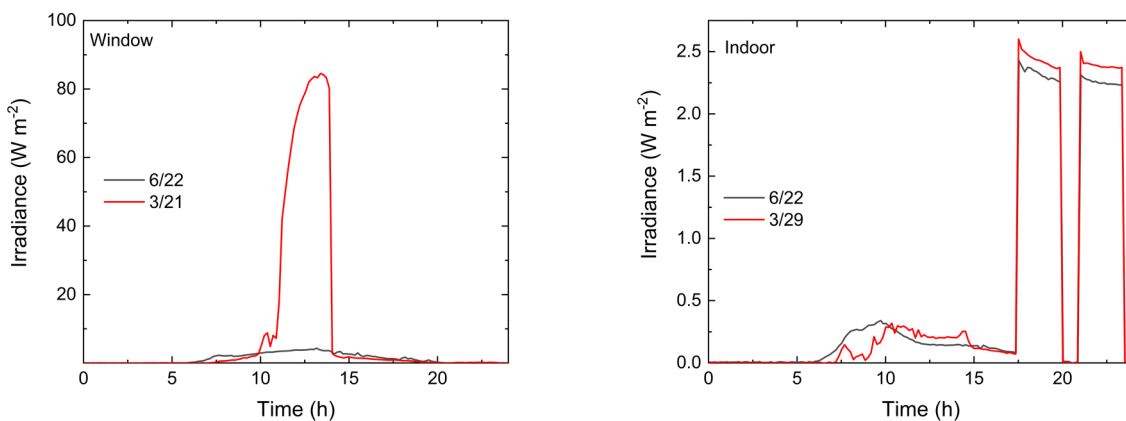


Figure 17. Total irradiance in the living room of NIST's Net-Zero Energy Residential Test Facility (NZERTF) at a) a south facing window and b) 50 cm under a recessed ceiling LED. Irradiance is reported on a day near the spring equinox (3/21) and a day near the summer solstice (6/22). Note that the roof overhang at the NZERTF reduces solar radiation incident on the windows during the summer and maximizes it during the winter months. LED lights turn on at time 17.5 h after midnight, which account for the peaks on the interior plot (right, note the difference in scale).

Outdoor solar spectral data was measured with spectroradiometer with a range of 300 nm to 1700 nm deployed on a rooftop weather station. Figure 18 shows the indoor and outdoor spectral data for sunny days near the spring equinox (3/18 and 3/24) and summer solstice (6/16). The solar spectrum generally scales depending on the irradiance and sun angle. The window filters out all radiation below 375 nm and reduces transmission in the visible and near infrared region. In total, the window appears to reduce total irradiance by a factor of 10 based on the change in integrated irradiance values and spectral intensities shown in Figure 18 (a). For comparison, Figure 18 (b) shows the same window data from Figure 18 (a) during a sunny spring equinox day and the spectral data at night while the ceiling LED light is on (green line). The bounded integrated irradiance of the diffuse light during the late morning (blue line) is still an order of magnitude smaller than that of the ceiling light. The interior of the living room (blue line) rarely sees maximum intensities above 0.5 W m^{-2} .

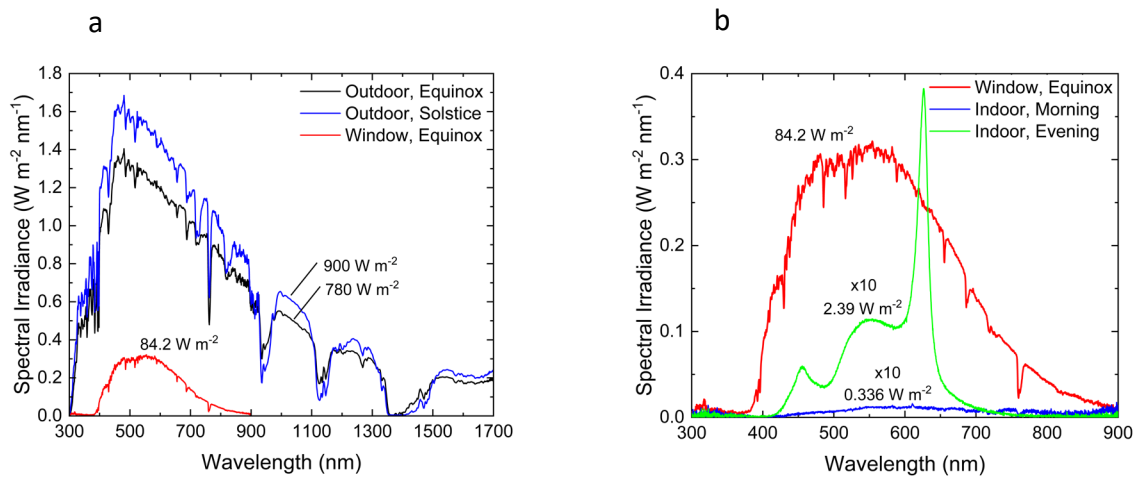


Figure 18. Measured spectral irradiance at various locations. The maximum irradiance due to solar radiation is shown in a) for outdoor conditions at peak irradiance near the spring equinox and summer solstice as well as on a peak day in spring equinox in the living room at a south facing window. This indoor window spectrum is also compared in b) to indoor spectra at night under the recessed LED and a peak measurement during the day while the LED is off.

5.2. Indoor Spatial and Temporal Total Irradiance Data Files

Data files are available upon request for sunny days near the spring equinox and the summer solstice recording the spectral irradiance measured at the window inside the NZERTF living room and underneath a ceiling LED towards the center of the house. The corresponding wavelength is given in the first row and the time of day shown in hours is in the first column. Each row of data gives the measured spectrum for a given time of day.

6. Summary and Conclusions

The appropriate implementation of GUV technologies to reduce airborne pathogen transmission requires providing the space with a fluence rate that is high enough to inactivate pathogens but not so high as to significantly impact indoor air chemistry. However, accurately determining the average fluence rate in a space is difficult. As shown in Table 2, the fluence rate determined from three different methods for a single GUV222 lamp in an empty chamber varied by over 30 %. The fluence rate for the deployment of GUV222 in real world settings will be impacted by furniture, reflections, and occupants. A better understanding of actual fluence rates in real world deployments is needed to fully capture the impact of GUV on indoor air chemistry.

The fluence in a room is directly proportional to the indoor air chemistry impacts. If fewer photons are required to inactivate a pathogen, there will also be a smaller impact on the indoor chemistry. As such, a better understanding of required fluence rates for various pathogens is needed to accurately determine indoor air chemistry impacts of GUV devices.

In this work, at the fluence rates tested for both GUV254 and GUV222 lamps, measurable impacts on the indoor air (Table 3) in chamber studies were observed. Any impacts in the restroom field deployment of GUV254 on indoor air chemistry were not quantifiable using the equipment used in this study. We demonstrated that unintended and undesirable air byproduct formation is possible from the GUV222 installation, but we have also shown that this byproduct formation is highly dependent on variety of factors including oxidation precursor concentrations, number of lamps used, air change rates, and air mixing.

Table 3. Quantifiable GUV impacts on indoor chemistry.

Impact	GUV254		GUV222	
	Chamber	Field	Chamber	Field
Ozone			X	X
Formaldehyde	X		X	
VOC Oxidation Products			X	X
Ultrafine Particles	X		X	X
Direct Photolysis	X		X	

Therefore, to optimize the net benefit of GUV technologies on public health more studies of air quality impacts on real-world GUV installations are needed. The restroom experiment presented here is the only study, to date, performing a comprehensive analysis of air quality impacts of GUV in a possible real-world installation. With additional experimental data from real-world studies, chemical models can be developed to aid in a risk assessment that considers the disinfection benefit with possible disbenefits from air byproduct exposure.

References

- [1] Bueno de Mesquita, P. J.; Delp, W. W.; Chan, W. R.; Bahnfleth, W. P.; Singer, B. C. Control of airborne infectious disease in buildings: Evidence and research priorities. *Indoor air* **2022**, *32* (1), e12965.
- [2] ASHRAE. *241-2023 Control of Infectious Aerosols*; 2023. DOI: https://ashrae.iwrapper.com/ASHRAE_PREVIEW_ONLY_STANDARDS/STD_241_2023.
- [3] Fujimoto, N.; Nagaoka, K.; Tatsuno, I.; Oishi, H.; Tomita, M.; Hasegawa, T.; Tanaka, Y.; Matsumoto, T. Wavelength dependence of ultraviolet light inactivation for SARS-CoV-2 omicron variants. *Scientific Reports* **2023**, *13* (1), 1-7.
- [4] Eadie, E.; Hiwar, W.; Fletcher, L.; Tidswell, E.; O'Mahoney, P.; Buonanno, M.; Welch, D.; Adamson, C. S.; Brenner, D. J.; Noakes, C. Far-UVC (222 nm) efficiently inactivates an airborne pathogen in a room-sized chamber. *Scientific reports* **2022**, *12* (1), 4373.
- [5] Guo, K.; Pan, Y.; Chan, H. F. R.; Ho, K.-F.; Chen, C. Far-UVC disinfection of airborne and surface virus in indoor environments: Laboratory experiments and numerical simulations. *Building and Environment* **2023**, *245*, 110900.
- [6] Buonanno, M.; Welch, D.; Shuryak, I.; Brenner, D. J. Far-UVC light (222 nm) efficiently and safely inactivates airborne human coronaviruses. *Scientific Reports* **2020**, *10* (1), 1-8.
- [7] Welch, D.; Kleiman, N. J.; Arden, P. C.; Kuryla, C. L.; Buonanno, M.; Ponnaiya, B.; Wu, X.; Brenner, D. J. No evidence of induced skin cancer or other skin abnormalities after long-term (66 week) chronic exposure to 222-nm far-UVC radiation. *Photochemistry and Photobiology* **2023**, *99* (1), 168-175.
- [8] Sliney, D. H.; Stuck, B. E. A need to revise human exposure limits for ultraviolet UV-C radiation. *Photochemistry and Photobiology* **2021**, *97* (3), 485-492.
- [9] Brenner, D. J. Far-UVC light at 222 nm is showing significant potential to safely and efficiently inactivate airborne pathogens in occupied indoor locations. *Photochemistry and Photobiology* **2023**, *99* (3), 1047-1050.
- [10] Nardell, Edward A., et al. "Safety of upper-room ultraviolet germicidal air disinfection for room occupants: results from the Tuberculosis Ultraviolet Shelter Study." *Public health reports* 123.1 (2008): 52-60.
- [11] Nardell, Edward, Richard Vincent, and David H. Sliney. "Upper-room ultraviolet germicidal irradiation (UVGI) for air disinfection: A symposium in print." *Photochemistry and photobiology* 89.4 (2013): 764-769.
- [12] Reed, Nicholas G. "The history of ultraviolet germicidal irradiation for air disinfection." *Public health reports* 125.1 (2010): 15-27.
- [13] Peng, Z.; Miller, S. L.; Jimenez, J. L. Model Evaluation of Secondary Chemistry due to Disinfection of Indoor Air with Germicidal Ultraviolet Lamps. *Environmental Science & Technology Letters* **2022**, *10* (1), 6-13.
- [14] Park, S.; Won, Y.; Rim, D. "Formation and Transport of Secondary Contaminants Associated with Germicidal Ultraviolet Light Systems in an Occupied Classroom." *Environmental Science & Technology* **2024**, *58* (27), 12051–12061.
- [15] Walker, C. M., & Ko, G. (2007). Effect of ultraviolet germicidal irradiation on viral aerosols. *Environmental science & technology*, *41*(15), 5460-5465.

- [16] Allen, G. R., Benner, K. J., & Bahnfleth, W. P. (2021). Inactivation of pathogens in air using ultraviolet direct irradiation below exposure limits. *Journal of Research of the National Institute of Standards and Technology*, 126.
- [17] Tseng, C. C., & Li, C. S. (2005). Inactivation of virus-containing aerosols by ultraviolet germicidal irradiation. *Aerosol Science and Technology*, 39(12), 1136-1142.
- [18] Link, M. F.; Robertson, R.; Claflin, M. S.; Poppendieck, D. Quantification of Byproduct Formation from Portable Air Cleaners Using a Proposed Standard Test Method. *Environmental Science & Technology* **2024**, 58 (18), 7916-7923. DOI: <https://doi.org/10.1021/acs.est.3c09331>.
- [19] Graeffe, F., Luo, Y., Guo, Y., & Ehn, M. (2023). Unwanted indoor air quality effects from using ultraviolet C lamps for disinfection. *Environmental Science & Technology Letters*, 10(2), 172-178.
- [20] Blatchley III, E.R., Brenner, D.J., Claus, H., Cowan, T.E., Linden, K.G., Liu, Y., Mao, T., Park, S.J., Piper, P.J., Simons, R.M. and Sliney, D.H., 2023. Far UV-C radiation: An emerging tool for pandemic control. *Critical Reviews in Environmental Science and Technology*, 53(6), pp.733-753.
- [21] Görlitz, M., Justen, L., Rochette, P.J., Buonanno, M., Welch, D., Kleiman, N.J., Eadie, E., Kaidzu, S., Bradshaw, W.J., Javorsky, E. and Cridland, N., 2024. Assessing the safety of new germicidal far-UVC technologies. *Photochemistry and Photobiology*, 100(3), pp.501-520.
- [22] Link, M. F., Shore, A., Hamadani, B. H., & Poppendieck, D. (2023). Ozone generation from a germicidal ultraviolet lamp with peak emission at 222 nm. *Environmental science & technology letters*, 10(8), 675-679.
- [23] He, L., Weschler, C.J., Zhang, Y., Li, F., Bergin, M.H., Black, M. and Zhang, J., 2023. Ozone reaction products associated with biomarkers of cardiorespiratory pathophysiology. *American Journal of Respiratory and Critical Care Medicine*, 207(9), pp.1243-1246.
- [24] He, L., Weschler, C.J., Morrison, G., Li, F., Zhang, Y., Bergin, M.H., Black, M. and Zhang, J.J., 2024. Synergistic Effects of Ozone Reaction Products and Fine Particulate Matter on Respiratory Pathophysiology in Children with Asthma. *ACS ES&T Air*.
- [25] Burkholder, J.B., Sander, S.P., Abbatt, J.P.D., Barker, J.R., Cappa, C., Crouse, J.D., Dibble, T.S., Huie, R.E., Kolb, C.E., Kurylo, M.J. and Orkin, V.L., 2020. Chemical kinetics and photochemical data for use in atmospheric studies; evaluation number 19. Pasadena, CA: Jet Propulsion Laboratory, National Aeronautics and Space Administration, 2020.
- [26] Link, M. F., Farmer, D. K., Berg, T., Flocke, F., & Ravishankara, A. R. (2021). Measuring Photodissociation Product Quantum Yields Using Chemical Ionization Mass Spectrometry: A Case Study with Ketones. *The Journal of Physical Chemistry A*, 125(31), 6836-6844.
- [27] Buonanno, M., Kleiman, N.J., Welch, D., Hashmi, R., Shuryak, I. and Brenner, D.J., 2024. 222 nm far-UVC light markedly reduces the level of infectious airborne virus in an occupied room. *Scientific Reports*, 14(1), p.6722.
- [28] Narouei, F., Tang, Z., Wang, S., Hashmi, R., Welch, D., Sethuraman, S., Brenner, D. and McNeill, V.F., 2024. Effects of Germicidal Far-UVC on Indoor Air Quality in an Office Setting.
- [29] Sørensen, S.B., F. R. Dalby, S. K. Olsen, K. Kristensen. Influence of Germicidal UV (222 nm) Lamps on Ozone, Ultrafine Particles, and Volatile Organic Compounds in Indoor Office Spaces. *Accepted Environmental Science and Technology*. 2024.

- [30] Deal, A.M. and Vaida, V., 2023. Oxygen effect on the ultraviolet-C photochemistry of lactic acid. *The Journal of Physical Chemistry A*, 127(13), pp.2936-2945.
- [31] Peng, Z., Day, D.A., Symonds, G.A., Jenks, O.J., Stark, H., Handschy, A.V., de Gouw, J.A. and Jimenez, J.L., 2023. Significant production of ozone from germicidal UV lights at 222 nm. *Environmental Science & Technology Letters*, 10(8), pp.668-674.
- [32] Link, M.F., Robertson, R.L., Shore, A., Hamadani, B.H., Cecelski, C.E. and Poppendieck, D.G., 2024. Ozone generation and chemistry from 222 nm germicidal ultraviolet light in a fragrant restroom. *Environmental Science: Processes & Impacts*, 26(6), pp.1090-1106.

A. Appendix

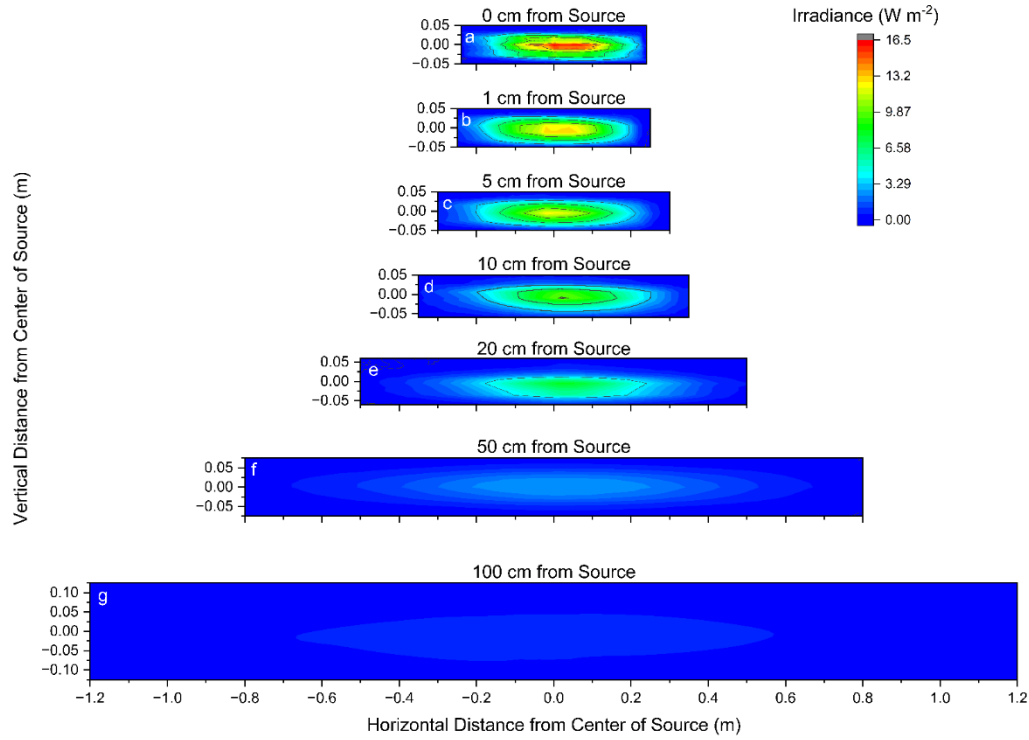


Figure A.1. Bounded Irradiance of 254 nm lamp measured in planes of a) 0 cm, b) 1 cm, c) 5 cm, d) 10 cm, e) 20 cm, f) 50 cm, and g) 100 cm from source. Irradiance values are integrated over 250 nm to 257 nm to capture emission at 254 nm. Irradiance color bar is kept constant for all measurements.

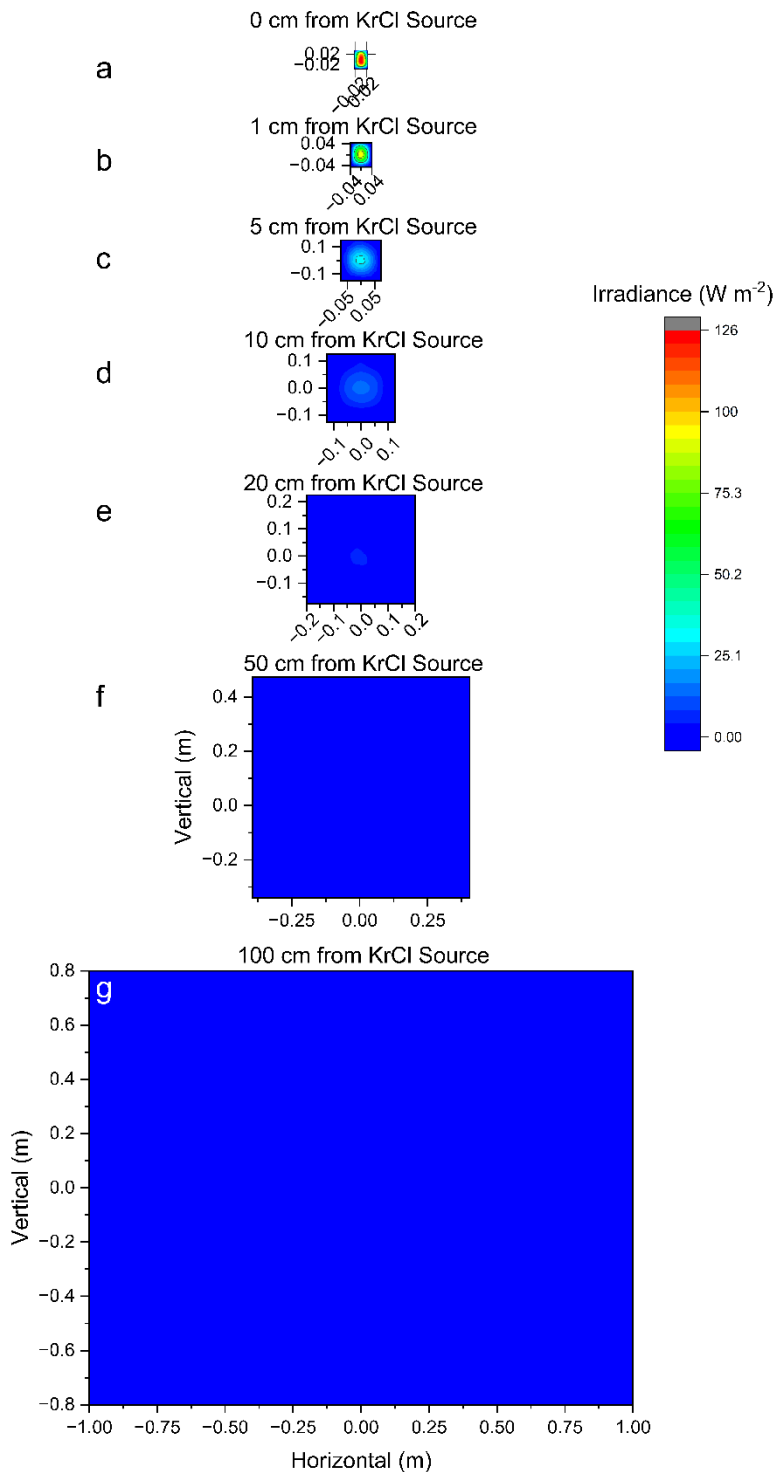


Figure A.2. Bounded Irradiance from KrCl 222 nm source measured in planes of a) 0 cm, b) 1 cm, c) 5 cm, d) 10 cm, e) 20 cm, f) 50 cm, and g) 100 cm from source. Irradiance values are integrated over 205 nm to 235 nm which gives the total emission of the lamp. Irradiance color bar is kept constant for all measurements.